ceramics

MDPI

Article

Modification of Sepiolite for Its Catalytic Upgrading in the Hydrogenation of Furfural

Antonio Guerrero-Torres [1], Rocío Maderuelo-Solera [1], Cristina García-Sancho [1,2], José J. Quirante-Sánchez [3], Ramón Moreno-Tost [1,2], Pedro J. Maireles-Torres [1,2] and Juan A. Cecilia [1,2,*]

[1] Departamento de Química Inorgánica, Cristalografía y Mineralogía, Facultad de Ciencias, Universidad de Málaga, Campus de Teatinos, 29071 Málaga, Spain; guerrerotorresantonio@gmail.com (A.G.-T.); rocioms@uma.es (R.M.-S.); cristinags@uma.es (C.G.-S.); rmtost@uma.es (R.M.-T.); maireles@uma.es (P.J.M.-T.)
[2] Instituto de Investigación en Biorrefinerías "I3B", Facultad de Ciencias, Universidad de Málaga, Campus de Teatinos s/n, 29071 Málaga, Spain
[3] Departamento de Química Física, Facultad de Ciencias, Universidad de Málaga, Campus de Teatinos, 29071 Málaga, Spain; quirante@uma.es
* Correspondence: jacecilia@uma.es

Abstract: In this work, a new methodology for dispersing metal particles supported in clay has been described. For this purpose, a sepiolite has been modified by a microwave-assisted treatment to increase the surface area and pore volume due to the progressive leaching of the Mg^{2+}-species located in the octahedral sheet. These materials have been used as support to incorporate Cu species on the surface by a precipitation-deposition process from the thermal decomposition of urea at 95 °C. Once calcined and reduced, the Cu-based catalysts showed a Cu^0-particle size lower than 5 nm in the case of catalysts whose support is a sepiolite subjected to acid treatment. On the other hand, when raw sepiolite is used as a support, the Cu^0-crystal size is much larger (15–20 nm). This difference in Cu^0-crystal size showed a variable catalytic behavior for the hydrogenation reaction of furfural in gas-phase. Catalysts with larger particle size promote the hydrogenation reaction, obtaining a yield towards furfuryl alcohol close to 60% after 5 h at 190 °C. In contrast, catalysts with smaller particle size promote the hydrogenation reaction and subsequently the hydrogenolysis reaction, obtaining methylfuran as a product with a yield of 58% after 1 h of reaction at 190 °C; however, the sites where hydrogenolysis are involved are more prone to be deactivated.

Keywords: Cu-based catalysts; supported sepiolite; acid treatment; furfural hydrogenation; furfuryl alcohol; methylfuran

check for updates

Academic Editors: Maurice Gonon, Sandra Abdelouhab and Gisèle Laure Lecomte-Nana

Received: 3 January 2025
Revised: 10 February 2025
Accepted: 18 February 2025
Published: 25 February 2025

Citation: Guerrero-Torres, A.; Maderuelo-Solera, R.; García-Sancho, C.; Quirante-Sánchez, J.J.; Moreno-Tost, R.; Maireles-Torres, P.J.; Cecilia, J.A. Modification of Sepiolite for Its Catalytic Upgrading in the Hydrogenation of Furfural. *Ceramics* **2025**, *8*, 21. https://doi.org/10.3390/ceramics8010021

Copyright: © 2025 by the authors. Licensee MDPI, Basel, Switzerland. This article is an open access article distributed under the terms and conditions of the Creative Commons Attribution (CC BY) license (https://creativecommons.org/licenses/by/4.0/).

1. Introduction

Phyllosilicates are a subclass of silicates with layered structure, which have been used in a wide range of research fields [1]. Among them, one of the most widely used phyllosilicates is sepiolite [2]. Around half of the world reserves of this clay mineral is in Spain, although there are notable deposits in Turkey, Morrocco, Greece and the United States [3]. The greatest significance of this clay mineral lies in its fibrous morphology due to the periodical inversion of its tetrahedral sheet leading to nanocavities with dimensions of 1.06 nm × 0.37 nm [4,5]. These nanocavities can host small molecules or cations to counter-balance the charge deficiency [4,6]. Sepiolite can be used, under appropriate pretreatments, as adsorbent, deodorant, filter air, catalytic support, decolorizing agent, additive in paints, anticaking agent, drilling fluids, cosmetics, detergents, asphalt coating, animal nutrition, agriculture, and for phytosanitary and pharmaceutical uses [2,5,7–11].

A strategy to modify the structure of sepiolite is through acid treatment [12–15]. Using this treatment, it is possible to significantly improve its textural properties due to a partial leaching of Mg^{2+} species located in the octahedral layer [12]. The acid treatment was performed with concentrated solutions for many hours, even days [13,14]. However, it has recently been shown that microwave-assisted treatment can reduce this time to a few minutes, using solutions that are an order of magnitude more dilute [12]. The characterization of sepiolite modified with acid treatment has been widely studied [12–15]. However, its application has been primarily limited to CO_2 capture processes [6] photocatalysis [16] and cementitious materials [17].

The interest in this acid treatment is related to a partial leaching of the octahedral layer, which produces an increase in the specific area and pore volume but also modifies its chemical properties due to the loss of Mg^{2+}-species of its octahedral sheet causing vacancies in the fibrous structure [12]. Considering these premises, modified sepiolite could be an interesting material to be studied as a catalytic support with high available surface area to disperse a certain active phase.

The model reaction carried out for this study has been the furfural (FUR) hydrogenation in gas phase. This reaction has been selected since FUR molecule is considered a building block molecule since it is possible to obtain a high range of valuable products from several reactions [18,19]. FUR is obtained from lignocellulosic biomass, specifically from the hemicellulose fraction, which is a polymer consisting of pentosans, mainly xylose [20]. In turn, xylose is dehydrated to obtain FUR [21]. FUR is considered the second most produced product in the sugar platform, after bioethanol. From FUR, advanced products used in the polymer field, fuel additive, fine chemical, fragrances, paints among others have been obtained [21,22]. Most FUR is preferably treated by reduction processes using transition metals as active phase [22], although other reactions have also been carried out to obtain high added value products [18,19].

Industrially, FUR reduction has been carried out with copper chromite as a catalyst [23–26]. However, restrictive environmental regulations have led to the scientific community developing new Cr-free catalysts. In this sense, Cu-based catalysts are the most inexpensive active phase to be implemented on a large scale [22]. This active phase only promotes the reaction with the carbonyl group, obtaining furfuryl alcohol (FOL) and 2-methylfuran (MF) as products [27,28]. Both compounds are considered high value-added products, as FOL is used in the polymer industry for its excellent thermochemical properties, while MF can be used as a fuel additive [29]. Previous studies have reported that the interaction between FUR and Cu-based catalysts plays an important role in the activity and the catalytic behavior [28]. Thus, several authors have proposed the use of a neutral or basic support to obtain higher conversion and stability, minimizing the formation of carbonaceous deposits [30–33]. In the same way, the presence of small Cu^0-crystals as active phase also promotes the formation of MF through a hydrogenolysis reaction [30,34–36]. Considering these assumptions, this work aims to analyze the influence of the modification of the support, through a microwave-assisted acid treatment in a sepiolite, on the active phase-support interaction and in turn on the size of the copper crystals. Likewise, this work also studies how these modifications of the support influence the catalytic behavior in the hydrogenation reaction of FUR in the gas phase.

2. Materials and Methods

2.1. Synthesis of Cu-Based Catalysts

Sepiolite, selected as support, was supplied by Tolsa S.A and marketed as Pangel S9. This fibrous phyllosilicate was collected in Vallecas deposits (Madrid, Spain) and was used without a prior treatment.

For each microwave-assisted acid treatment, 5 g of sepiolite was suspended in a solution of 50 mL HNO_3 (0.2 M). Then, each sample was subjected to microwave radiation in a commercial microwave system EMS20100OX (Electrolux, Stockholm, Sweden) using an open glass cylinder reactor, operating at 800 W and 2.45 GHz for between 1 and 16 min. According to previous studies, the microwave radiation was discontinuously applied to avoid a temperature above 100 °C. Thus, once the sample was irradiated for 1 min, then, the suspension was cooled for 5 min [12,37,38]. This procedure was repeated until the desired radiation time was reached. Once the microwave-assisted treatment was performed, the sample was centrifuged and washed several times to remove NO_3^- species used in the acid treatment. Following this methodology, previous studies have described that the octahedral layer is progressively dissolved in magnesian phyllosilicates [12,37,38].

The Cu species were deposited on the surface of the sepiolite using copper nitrate trihydrate $Cu(NO_3)_2{\cdot}3H_2O$ (Sigma-Aldrich, Darmstadt, Germany, 99%) as copper source and urea as precipitant agent. Thus, for each synthesis, 2 g of the raw sepiolite or sepiolite subjected to the microwave-assisted acid treatment was suspended in 6 g of urea and the appropriate amount of $Cu(NO_3)_2{\cdot}3H_2O$ to obtain catalysts with a Cu loading between 5 and 20 wt.%. Later, the suspension was heated at 95 °C for 2 h to promote thermal decomposition of urea into CO_2 and NH_3, which promotes the precipitation and deposition of the Cu species on the surface of the sepiolite. In the next step, the solid was filtered, discarding the presence of Cu species in the solution. Then, the samples were washed with distilled water two times and dried at 90 °C overnight. Finally, the solid was calcined at 400 °C for 2 h and reduced to the desired temperature considering their respective H_2-TPR profiles.

The uncalcined samples were labeled as Prec-XCuO-Sep-Y, the calcined samples XCuO-Sep-Y and the reduced samples were labeled has XCu-Sep-Y where X indicates the Cu content in wt.%, while Y indicates the time of microwave-assisted acid treatment at which was subjected the sepiolite.

2.2. Characterization Techniques

Crystallinity of the samples was determined by X-Ray diffraction (XRD). The chemical composition of the samples was carried out by X-Ray fluorescence (XRF), attenuated total reflectance (ATR) and diffuse reflectance spectroscopy. The morphology of the catalysts was studied by Transmission Electron Microscopy (TEM). The analysis of the textural properties was evaluated from the analysis of their N_2 adsorption–desorption isotherms at −196 °C. The superficial charge of the modified sepiolites was performed by the analysis of their zeta-potential. The analysis of the chemical composition of the surface of the catalyst was performed by X-ray photoelectron spectroscopy (XPS). The reducibility of the Cu-based precursors was carried out by the analysis of their H_2-thermoprogrammed reduction (H_2-TPR) profiles. The detailed description of each characterization technique is provided in the Supplementary Material.

2.3. Catalytic Studies

The hydrogenation of FUR has been performed in a vapor-phase atmospheric-pressure fixed-bed continuous flow quartz catalytic reactor with a diameter of 6.35 nm. Prior to each study, the samples were pelletized with a range of 215–400 μm. The sample was placed in the middle of the quartz reactor, being retained with two layers of quartz wool. The temperature was controlled with a thermocouple, which was inserted in the quartz reaction, being in direct contact with the fixed bed. Prior to each study, the precursor was reduced under H_2-flow, following the H_2-TPR profiles studied previously. This temperature was

maintained for 1 h to ensure the total reduction in the Cu^{2+}-species to Cu^0. After the reduction, the catalyst was cooled until the selected temperature.

FUR was pumped with a Gilson 307SC piston pump (model 10SC) with a flow of 3.87 mL/h of a FUR solution in CPME (5 vol.%) to reach a weight hourly space velocity (WHSV) for FUR of 1.5 h^{-1} with a flow of 10 mL/min.

Both reagents and products were quantified in a Shimadzu GC-14B gas chromatograph equipped with a flame ionization detector (FID) and a CP-Wax 52CB capillary column. The furfural conversion and product selectivity were calculated as follows:

$$Conversion\ (\%) = \frac{mol\ of\ furfural\ converted}{mol\ of\ furfural\ fed} \times 100 \quad (1)$$

$$Selectivity\ (\%) = \frac{mol\ of\ product}{mol\ of\ furfural\ fed} \times 100 \quad (2)$$

3. Results and Discussion

Characterization of the Catalysts

Prior to the synthesis of the catalysts, the raw sepiolite was subjected to a microwave-assisted acid treatment with a range of time between 1 and 16 min. Figure 1 compiles some representative diffractograms of the sepiolite after this treatment. The diffractogram of the raw sepiolite reveals that the starting material displays high purity (PDF N: 98-015-6199), discarding the presence of impurities [12,39]. Microwave-assisted acid treatment causes a clear change in the diffraction profile, which becomes more pronounced as the treatment time increases. Thus, (110) reflection decreases clearly while the set of reflections located between 2θ (°) of 15–40 also decrease noticeably, forming a very broad and poorly defined signal, which is attributed to the formation of amorphous silica [12,40].

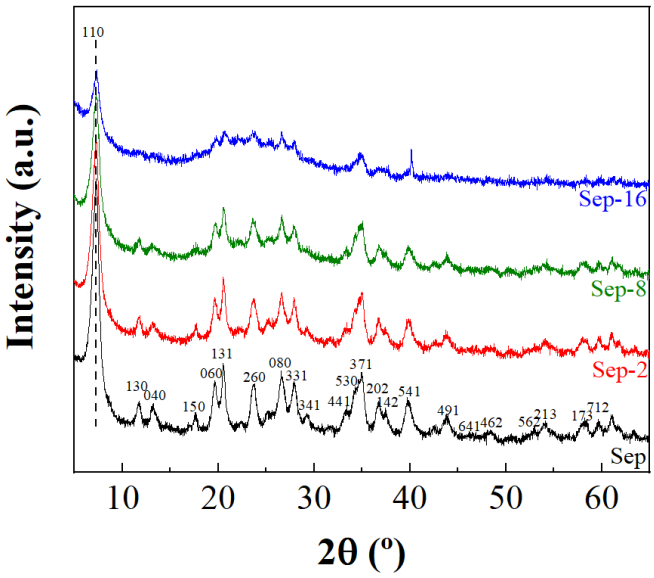


Figure 1. X-ray diffractograms of the raw sepiolite and sepiolite subjected at different times of microwave-assisted acid treatment.

The chemical composition of the raw clay and those samples subjected to microwave-assisted acid treatment was determined by XRF (Figure 2 and Supplementary Material, Table S1). These data reveal how the raw clay is mainly composed of Si and Mg, which suggests the presence of a trioctahedral clay such as sepiolite. After the microwave-assisted acid treatment, the Mg content notably decreases while the Si-content increases progressively. These data confirm that Mg species located in the octahedral sheet of sepiolite

is partially leached, leading to the formation of a silicious material with poorer crystallinity, as was suggested by XRD (Figure 1).

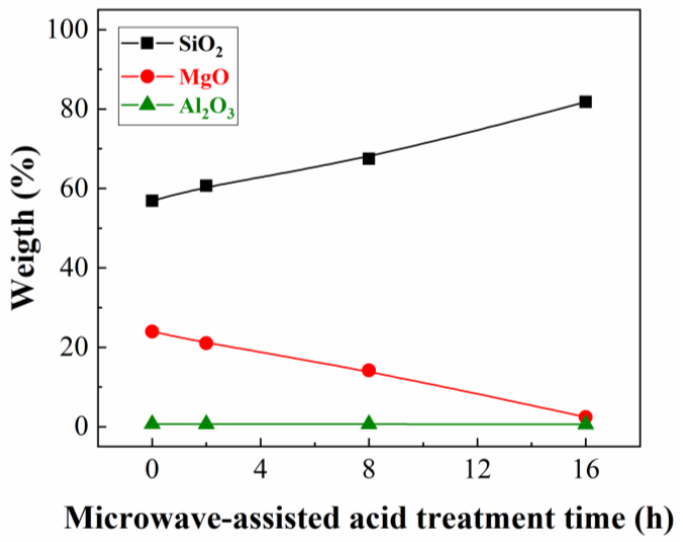


Figure 2. Evaluation of the SiO_2, MgO and Al_2O_3 with the microwave-assisted acid treatment. (Data obtained from XRF).

Infrared spectroscopy has also been used to study how the acid treatment affected the sepiolite. As can be seen in Figure 3, this treatment causes changes in the spectrum of the starting sepiolite. In the region between 4000 and 3000 cm^{-1}, the sepiolite shows different bands associated with the stretching vibrations of the -OH group, such as the bands at 3687 cm^{-1} associated with the stretching of the OH bound to octahedral Mg^{2+} (Mg_3OH) [41], the band at 3618 cm^{-1} associated with the Si-OH groups [41], the band at 3566 cm^{-1} associated with structural water [41] and the band at 3369 cm^{-1} associated to zeolitic water [41]. The intensity of these bands is modified, and some of them even disappear, with the acid treatment [12,37]. Thus, the bands associated with the vibrations of the -OH groups associated with Mg^{2+} disappear, at 3687 and 3566 cm^{-1}, which would indicate the solubilization of the octahedral layer with the treatment time, while the bands due to the Si-OH groups and adsorbed water remain [12,37]. These changes are corroborated when analyzing the bands due to the sepiolite structure in the region between 1400 and 400 cm^{-1} [12,41]. In this region, the bands corresponding to the vibrations of the Si-O bonds remain, such as the bands at 1213, 1078 and 976 cm^{-1}, corresponding to the Si-O bond in the tetrahedral sheet [41], the Si-O-Si vibration at 1004 cm^{-1} [41] and the band at 791 cm^{-1} corresponding to the symmetrical strain of the Si-O-Si group [41], while the bands associated with octahedral Mg^{2+} disappear at 689 and 642 cm^{-1}, corresponding to the bending of the OH group in Mg_3OH and attached to octahedral Mg^{2+} [41,42], respectively. As the acid treatment time increases, the bands due to the Si-O bonds become wider and less defined, indicating an increase in the amorphization of the sepiolite [4,5].

The determination of the textural properties of the raw sepiolite and sepiolite subjected to microwave-assisted acid treatment was carried out through their N_2 adsorption–desorption isotherms at −196 °C (Table 1 and Supplementary Material, Figure S1). According to the IUPAC classification, all isotherms can be adjusted to type II [43], which are typical of microporous materials; although, the high N_2-adsorption at low relative pressure suggests that these materials also display microporosity [43]. These data agree with those reported in the literature previously where the periodic inversion of its tetrahedral sheet leads to the formation of nanocavities of 1.06 nm × 0.37 nm [4,5], which is related to the microporosity of this fibrous phyllosilicate [6]. On other hand, all samples

hardly display hysteresis loops, which confirms a pore diameter lower than 4 nm [43]. The analysis of the N_2 adsorption–desorption isotherms reveals that the microwave-assisted acid treatment promotes a progressive increase in the N_2-adsorbed at low and intermediate relative pressures because of the Mg-leaching of the octahedral sheet causes an increase in the nanochannels.

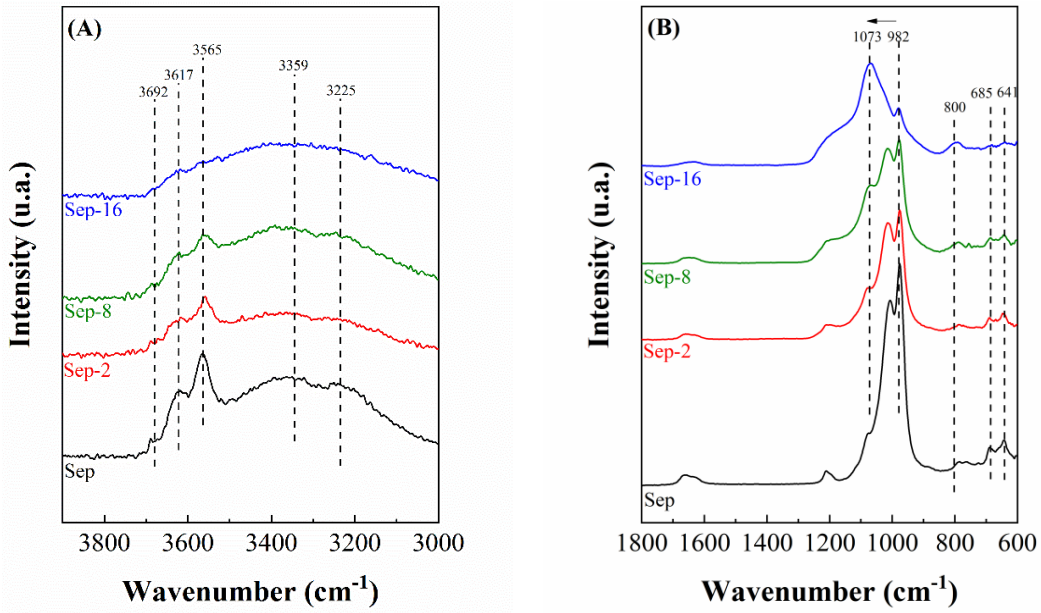


Figure 3. ATR of the raw sepiolite and sepiolite subjected at different times of microwave-assisted acid treatment. Wavenumber region 3900–3000 cm^{-1} (**A**) and wavenumber region 1800–600 cm^{-1} (**B**).

Table 1. Textural properties obtained from the N_2 adsorption–desorption isotherms at −196 °C for the raw sepiolite and sepiolite subjected to different times of microwave-assisted acid treatment.

Sample	S_{BET} (m^2/g)	t-Plot (m^2/g)	S_{ext} (m^2/g)	V_p (cm^3/g) [1]	V_{mp} (cm^3/g) [2]
Sep	283	149	134	0.3678	0.1382
Sep-1	333	160	173	0.4345	0.1609
Sep-2	347	155	192	0.4513	0.1736
Sep-4	370	175	195	0.4904	0.1813
Sep-8	452	246	206	0.5312	0.2164
Sep-12	468	244	224	0.5512	0.2246
Sep-16	509	266	243	0.5959	0.2421

[1] V_p: Pore volume. [2] V_{mp}: Micropore volume.

The quantification of the surface area determined by the BET equation [44] (Table 1) shows how the microwave-assisted acid treatment causes an increase in the surface area from 283 m^2/g to 509 m^2/g after 16 min of microwave-assisted acid treatment. In the same way, the microporosity and the external surface improve after this time. On the other hand, the analysis of the pore volume follows a similar trend since the porosity rises notably after the microwave-assisted acid treatment. The increase in the surface area and pore volume is attributed to the progressive leaching of the Mg species as well as the amorphization of the remaining silica [12,37]. The analysis of the pore size distribution (Supplementary Material, Figure S2) reveals that the microwave-assisted acid treatment mainly affects the micro- and mesoporosity, as indicated by the shift in the pore size distribution at higher values, while the macroporosity is hardly modified. This suggests that acid treatment on sepiolite may take place either across the fiber edges in the octahedral

sheet or in the nanocavities formed by periodical inversion of the tetrahedral layer [45], causing an increase in the micro- and mesoporosity.

As the textural properties and chemical composition of sepiolite are modified along the microwave-assisted acid treatment, the next was the determination of the point of zero charge for the raw sepiolite and those samples modified by acid treatment. The data reported in the Supplementary Material, in Figure S3, show that the microwave-assisted acid treatment causes a shift in the point of zero charge at lower pH values when Mg species are progressively extracted from the octahedral layer of sepiolite, confirming the chemical modifications of this fibrous clay after the treatment. The study of the samples at higher pH values indicates that the samples where the Mg^{2+}-species have been partially extracted (Figure 2 and Supplementary Material, Table S1) are those samples with a higher content of negative charges in their structure.

After characterizing the raw sepiolite and the sepiolite subjected to microwave-assisted acid treatment at different times, the incorporation of Cu species on the supports with different composition was carried out following the methodology of thermal decomposition of urea, where the presence of NH_3 favors the precipitation of the Cu species.

This methodology was chosen because the decomposition of urea favors the formation of more homogeneous metallic particles because of a more homogeneous increase in pH compared to other methodologies where basic solutions were added [46]. The study of the Prec-15CuO-Sep-Y samples by XRD (Figure 4) reveals that this treatment hardly modifies the crystallinity of the supports. It is striking that Cu species are only observed in the Prec-15CuO-Sep, appearing to reflections located at 2θ (°) of 35.2 and 38.4, which are assigned to the presence of CuO (PDF N. 01-089-2531). However, those samples where sepiolite modified by acid treatment is used as support do not show diffraction peaks assigned to Cu species.

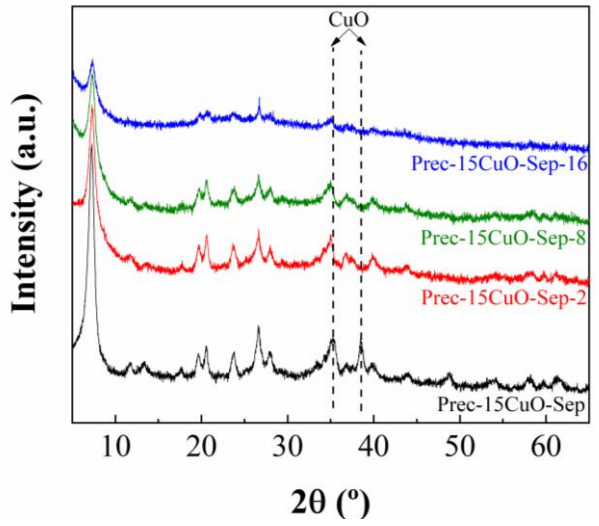


Figure 4. X-ray diffractograms of the raw sepiolite and sepiolite subjected at different times of microwave-assisted acid treatment with Cu species deposited on its surface.

During synthesis, urea hydrolysis provides the necessary hydroxide ions, derived from the acid-base equilibrium of released ammonia, for $Cu(OH)_2$ formation [47]. In the presence of nitrate ions, this leads to Cu(II) hydroxide nitrate formation ($Cu_2(OH)_3NO_3$), as nitrate ions have a strong tendency to incorporate into the $Cu(OH)_2$ crystal structure [48]. This compound has been confirmed through XRD (Supplementary Material, Figure S4) by precipitating it following the experimental procedure described above, leading to $Cu_2(OH)_3NO_3$ as the only crystalline phase (PDF N: 00-045-0594). This $Cu_2(OH)_3NO_3$ consists of positively charged layers with $Cu_2(OH)_3^+$ stoichiometry, neutralized by nitrate ions in the interlayer

space [47]. Due to the basic synthesis medium, the sepiolite surface becomes activated through the reaction of its surface hydroxyl groups with hydroxide anions, allowing the surface to become negatively charged and thus interact with $Cu_2(OH)_3NO_3$. On the other hand, upon filtering, a dark solid was obtained, indicating that $Cu_2(OH)_3NO_3$ likely did not exist on the sepiolite surface, as confirmed by XRD analysis. Additionally, XPS analysis (Supplementary Material, Table S1) confirmed the absence of $Cu_2(OH)_3NO_3$, as the surface N content in sepiolite was negligible (Supplementary Material, Figure S5). The appearance of CuO instead of $Cu_2(OH)_3NO_3$ on the surface may be due to its decomposition under reaction conditions. The synthesis temperature (95 °C) likely promotes this decomposition to CuO, which is the phase detected on untreated sepiolite. Van der Grift et al. [49] indicated that when solution pH exceeded 6.8 at 90 °C, $Cu_2(OH)_3NO_3$ became unstable and decomposed, depositing as hydrated octahedral Cu(II) on SiO_2, rather than as CuO as in our case. Lee et al. [50] showed that $Cu_2(OH)_3NO_3$ or CuO formation depended on both $[OH^-]/[Cu(NO_3)_2]$ ratio and temperature.

Regarding acid-treated sepiolite, for any treatment duration, all showed a blue-green color after Cu(II) deposition, indicating that CuO formation was not favored, but rather Cu(II) likely deposited as isolated Cu(II) ions or forming small aggregates on the support (Supplementary Material, Figure S6). In this case, XRD only showed peaks ascribed to treated sepiolite with no other phases detected. XPS analysis showed no detectable N quantity, as with untreated sepiolite, ruling out Cu(II) species having N-containing compounds like ammonia or nitrate in their coordination sphere (Supplementary Material, Figure S5). The acid treatment removed $Mg(OH)_2$ from sepiolites, exposing the tetrahedral SiO_2 layers of sepiolite. Cu catalyst synthesis on SiO_2 was studied by Toupance et al. [51–53], evaluating the Cu species present. Their method, termed "cation exchange" or "selective adsorption", involved the synthesis of the octhaedral $[Cu(NH_3)_4(H_2O)_2]^{2+}$ complex and suspending SiO_2 in a complex solution maintaining pH above 9 to avoid $Cu_2(OH)_3NO_3$ precipitation. They observed two distinct species on SiO_2: isolated Cu species, $(\equiv SiO)_2Cu(NH_3)_2(H_2O)_2$, and Cu phyllosilicate formation. They proposed Cu phyllosilicate formation occurred in solution, as at basic pH, silica dissolved as $Si(OH)_4$ and condensed with neutral $[Cu(OH)_2(H_2O)_4]^0$ species. These species were more abundant at pH 9, while Cu(II) tetraamine complex was more abundant at higher pH. The authors demonstrated that bridging -OH ligands were necessary for phyllosilicate formation, while ligands like ammonia or ethylenediamine prevented it. Additionally, neutral Cu species were necessary for phyllosilicate formation as they could condense to form a solid phase. Considering this background, we can postulate that acid-treated sepiolite, in the catalyst synthesis medium, may have partially dissolved silica as silicic acid, which would condense with $Cu_2(OH)_3NO_3$ species forming Cu phyllosilicate on the sepiolite surface.

In order to analyze the chemical composition of the obtained materials on their surface, XPS experiments were carried out (Figure 5 and Supplementary Material, Table S2). The analysis of the different core level spectra confirms the typical bands of their respective oxides. The acid treatment hardly causes a shift in the binding energy values in each region. However, the analysis of the Mg 1s core level spectra confirms that the Mg content progressively decreases from 10.12% until 0.74% after 16 min of treatment (Supplementary Material, Table S2). This decrease was accompanied by an increase in the Si-content, confirming the formation of a SiO_2-rich material with prolonged acid treatment. The analysis of the Cu 2p core level spectra shows a main contribution with a maximum about 933.2 eV for Prec-15CuO-Sep while the Cu-based materials subjected to a microwave-assisted acid treatment the contribution appears about 935.0 eV. In both cases, this contribution is ascribed to the presence of Cu(II)-species. In the same way, the presence of a broad band located about 942 eV, attributed to the shake-up satellite, confirms the presence of Cu

as a divalent species. The shift in the binding energy for those samples subjected to the acid treatment must be related to a modification of the interaction of the Cu(II)-species with the support by the formation of a Cu phyllosilicate on the surface of the sepiolite subjected to the acid treatment. The analysis of the atomic concentration on the surface of the catalysts reveals that Prec-15CuO-Sep sample displays lower amount of Cu species on the surface (Supplementary Material, Table S2). According to the XRD data (Figure 4), the lowest level of Cu species in this sample must be ascribed to Cu(II) species with higher agglomeration. The analysis of the N-content on the surface of the precursors is similar in all cases 0.31–0.39%, discarding the deposition of nitrate species and/or the amine-Cu complex. These values are below those obtained for Cu on the surface by XPS. Thus, it is expected that the ammonia formed in the decomposition of urea produces a rise in pH. However, the diffraction and XPS data rule out the formation of Cu complexes on the surface, at least for the most part.

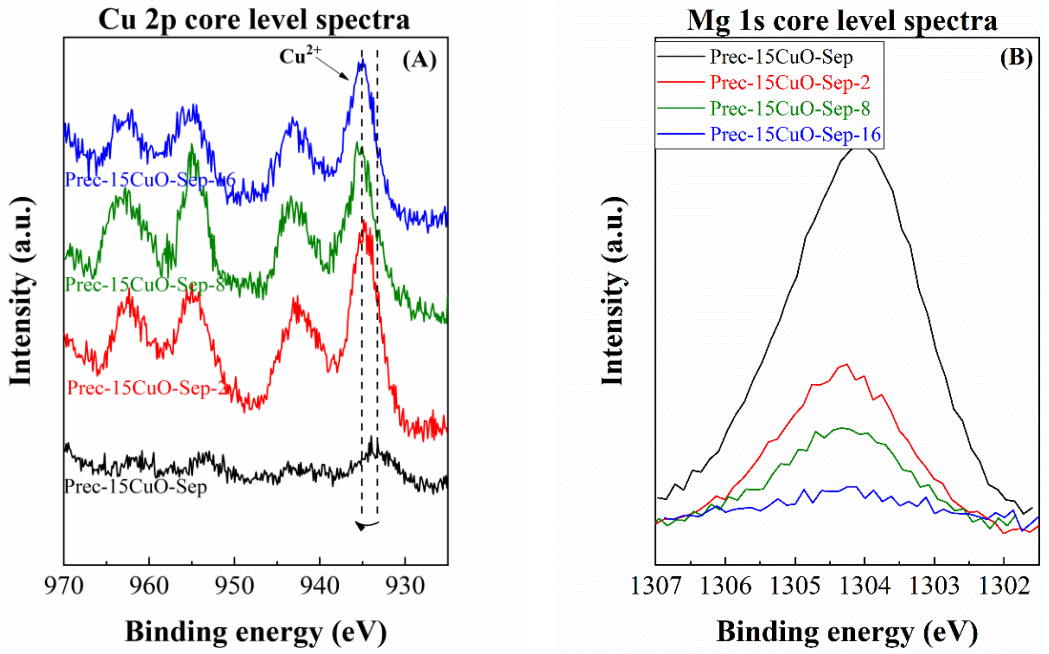


Figure 5. Cu 2p (**A**) and Mg 1s (**B**) core level spectra of the raw sepiolite and sepiolite subjected at different times of microwave-assisted acid treatment with Cu species deposited on its surface (estimated by XPS).

Once the samples were calcined, the precursors show similar colors. Thus, the 15CuO-Sep sample maintains a black color (Supplementary Material, Figure S7). However, the color evolves to green, for the same Cu content, as the microwave-assisted treatment time increases so the sintering during the calcination step must be ruled out.

Figure 6A shows the UV-vis spectra of Cu-based catalysts supported on sepiolite after acid treatment and calcination at 450 °C. These spectra show unequivocally that the Cu species present in the acid-treated sepiolite are completely different from those present in the untreated sepiolite. The latter shows bands 204, 206 and 299 cm^{-1} of charge transfer from the O^{2-} ligand to isolated Cu^{2+} ions [54], others at longer wavelengths (322 and 359 cm^{-1}) which are associated with oligomeric Cu species with different degrees of oligomerisation, indicating the presence of Cu-O clusters [55] and a broad band extending beyond 800 nm, as was observed by previous authors [55], due to d-d transitions of the Cu^{2+} ion in an octahedral environment, characteristic of bulk CuO particles [56]. As for Cu catalysts supported on sepiolite treated in acid medium, an intense broad band extending from 300 nm to approximately 700 nm can be distinguished, in which different contributions associated with Cu(II) species forming different cluster sizes are observed.

The magnification of this band may indicate a large tetragonal distortion of Cu(II) in these clusters increasing the intensity as they are less forbidden transitions by Laporte's rule [57]. For these catalysts, the absence of the band associated with the transitions due to CuO is remarkable, which would indicate a large dispersion of the CuO particles. The band gap increases significantly in the case of the catalysts based on sepiolite treated in acid medium, approximately 2 eV (Supplementary Material, Figure S8) with respect to the untreated one, which shows a modification of the copper species present in the catalysts and a lower semiconductor characteristic.

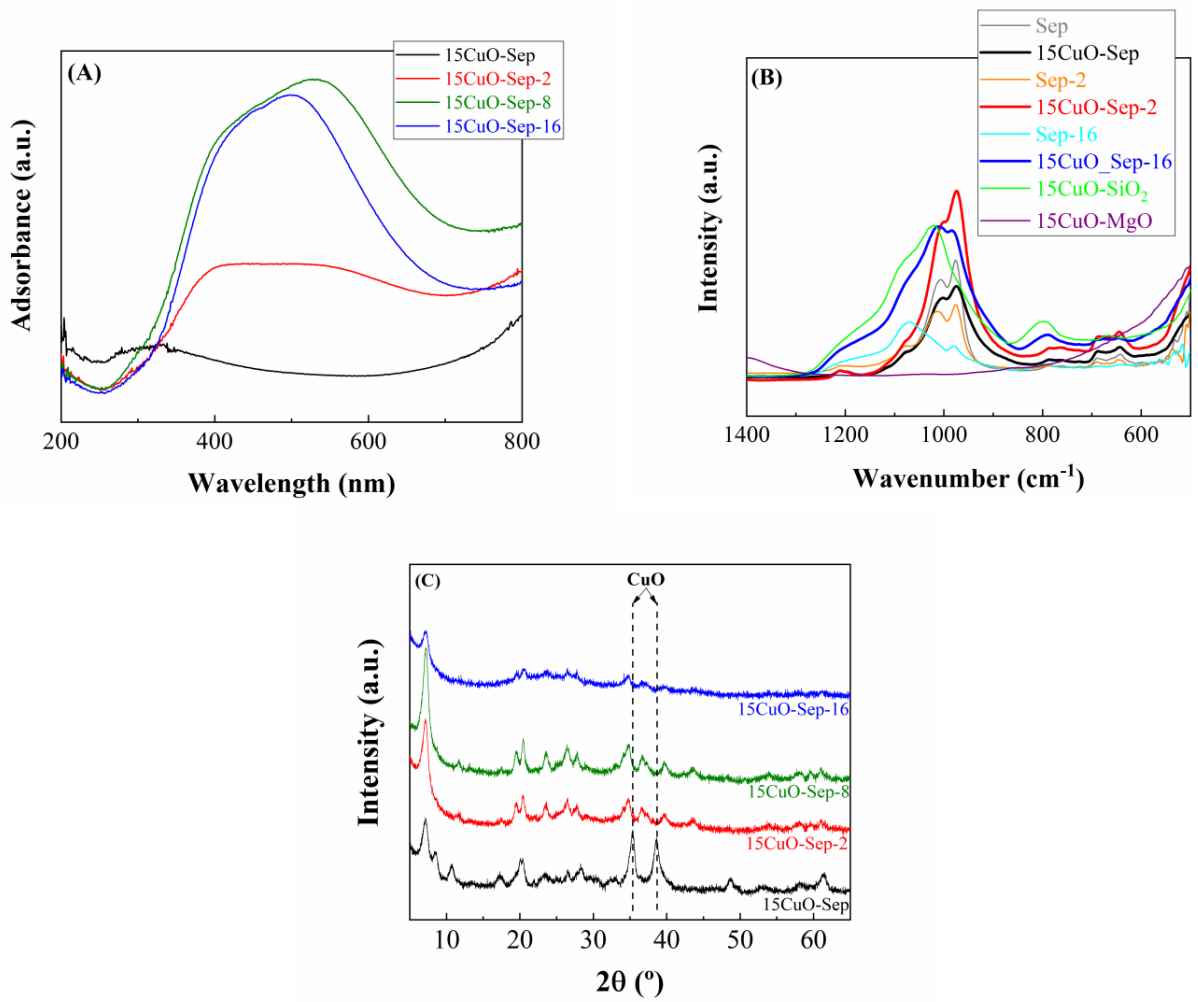


Figure 6. Diffuse reflectance spectra (**A**), ATR spectra (**B**) and XRD (**C**) of the raw sepiolite and sepiolite subjected at different times of microwave-assisted acid treatment with Cu species deposited on its surface and calcined at 450 °C.

When Cu^{2+} is incorporated into the untreated or acid-treated sepiolite, no remarkable changes are observed by ATR after Cu deposition (Figure 6B), both in the region of the hydroxyl group tension and in the region of the bands associated with the sepiolite structure. However, some bands have increased in intensity, such as the band at 974 cm^{-1}, which would indicate the formation of the Si-O-Cu bond [58]. It should also be noted that the bands associated with the Mg-OH bonds of the untreated sepiolite are recovered again in the case of the sepiolite treated for 16 min, which could indicate that Cu(II) occupies the sites left by the Mg(II). The presence of Cu phyllosilicate cannot be assured since the characteristic bands of this compound, above 1020–1030 cm^{-1} (ν_{Si-O}) and 675 cm^{-1} (δ_{OH}) are obscured by those due to Si-O or Mg-OH bonds [41,59]. The presence of $Cu(OH)_2$ could be ruled out by the absence of the bands at 938 and 694 cm^{-1} corresponding to δ_{OH}, as

well as the presence of Cu(II) oxynitrate, since the bands of the nitrate ion at 1423 and 1347 cm^{-1} are not observed [41,60]. Finally, the bands corresponding to CuO that should appear between 575 and 460 cm^{-1} are not observed, ruling out the presence of segregated CuO, as the XRD and UV-vis spectra demonstrated. As a conclusion, it could be indicated that Cu^{2+} is highly dispersed on the treated sepiolite forming Si-O-Cu.

The analysis of the calcined samples by XRD (Figure 6C) shows a decrease in the intensity of the reflections attributed to sepiolite, probably due to the thermal treatment causes a partial amorphization of the sepiolite. In the same way, the diffractograms also reveal that the reflections ascribed to Cu species in the form of CuO-crystals are only detected for the sample 15CuO-Sep, which suggests the formation of bigger crystals in this precursor. On the other hand, it is striking that the other precursors, which were subjected to microwave-assisted acid treatment, do not present reflections attributed to Cu species, confirming the high dispersion as well as good resistance to sintering after the thermal treatment at 450 °C for 2 h.

Once the supports and the precursors were characterized, the next step was the study of the reducibility of the Cu-based precursors by H_2-TPR (Figure 7). From the reduction profiles, it is not possible to discern the reduction steps $Cu^{2+} \rightarrow Cu^{+} \rightarrow Cu^{0}$. In this sense, previous authors have indicated that the reducibility is directly related to the interaction precursor-support and the crystal size of the precursor [61,62]. The data reported in Figure 7 shows how the reduction of 15CuO-Sep sample takes place between 150 and 350 °C while those catalysts where the support was subjected to a microwave-assisted acid treatment display a reduction in a narrower temperature range. These data suggest that 15CuO-Sep sample presents CuO-particles with variable particle size, which should affect its reducibility, while the particle size of the precursors, where the support was modified by an acid treatment, seems to be more homogeneous. On the other hand, the supports modified with acid treatment also display a maximum value of reducibility 20–30 °C lower than that observed for 15CuO-Sep sample. This shift supposes a poorer interaction between CuO and sepiolite which could be to the modification of the support because of the progressive loss of Mg in the sepiolite along the acid treatment (Figure 2 and Supplementary Material, Table S2. The H_2-TPR profiles also suggest that the presence of smaller CuO crystals promotes easier reducibility than that observed in 15CuO-Sep precursor where larger CuO clusters were obtained, as was observed by XRD (Figure 6C). Considering the H_2-TPR profiles, all Cu-based catalysts were reduced at 350 °C for 1 h to ensure a total reduction in the Cu species.

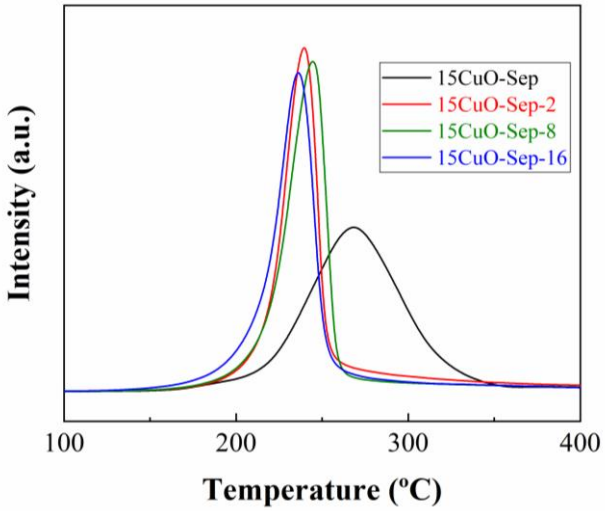


Figure 7. H_2-TPR profiles of the Cu-based precursors supported on raw sepiolite and sepiolite modified with microwave-assisted acid treatment at different times.

The analysis of the crystallinity of the Cu-based catalysts after its reduction (Figure 8) shows the typical reflection lines ascribed to sepiolite, which were described above. In addition, two new reflection lines located at 2θ (°) of 43.2 and 50.4° for 15Cu-Sep catalyst, which are ascribed to the formation of metallic copper (Cu^0) (PDF N°: 00-002-1225). However, the diffractograms of the other Cu-based catalysts, where sepiolite was treated with acid treatment, do not show diffraction peaks assigned to copper species, confirming a higher dispersion of Cu^0 for these catalysts after its reduction.

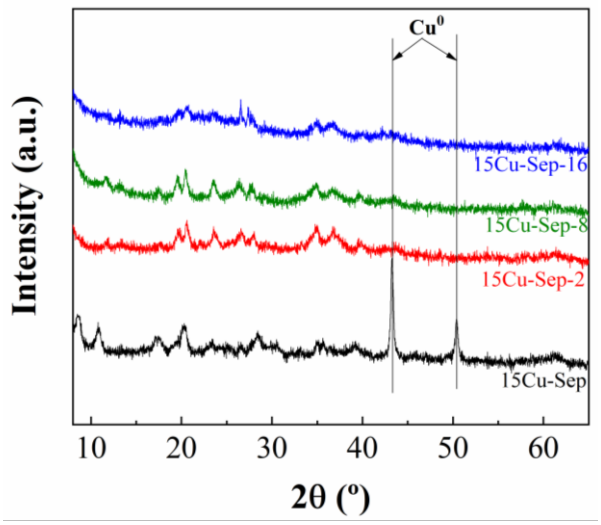


Figure 8. X-ray diffractograms of the Cu-based catalysts supported on raw sepiolite and sepiolite modified with microwave-assisted acid treatment at different times.

The morphology for the Cu-based catalysts was analyzed by TEM (Figure 9 and Supplementary Material, Figure S9). These micrographs reveal how the fibrous morphology of the sepiolite is progressively damaged due to the acid treatment causes a collapse of their structure by a progressive leaching of the Mg species located in the octahedral sheet. Regarding the Cu^0-particles, it is striking how all catalysts present metallic particles with spherical morphology, which are homogeneously dispersed on the surface of the sepiolite. However, the size of the metallic particles differs among them. Thus, the 15Cu-Sep catalyst displays a Cu^0 particle size between 15 and 25 nm (Figure 9A). However, those catalysts where the sepiolite was subjected to acid treatment (Figure 9B–D) show a lower Cu^0 particle size, being lower than 5 nm in all cases, confirming the data observed by XRD (Figure 8). The analysis of crystal size average shows how the modification of the sepiolite by microwave-assisted acid treatment is directly related to the dimensions of the Cu particles since the use of longer acid treatments promote smaller crystals after the calcination and reduction in the Cu species (Supplementary Material, Figure S10).

The analysis of the catalysts after their reduction by XPS shows how the spectra of each region are maintained, except in the Cu 2p core level, where the contributions attributed to the formation of CuO have disappeared. Thus, the Cu $2p_{3/2}$ region only shows a new contribution located about 932.6 eV, which is typical of reduced Cu species (Figure 10A). On the other hand, it is striking that 15Cu-Sep catalyst displays the main contribution at higher binding energy value. This shift is attributed to a change in the electronic charge density of the Cu^0 particles, which is related to the lower reducibility (Figure 7) and higher crystal size of the metallic particles in 15Cu-Sep catalyst (Figures 8 and 9). The analysis of the atomic concentration on the surface of the catalyst (Table 2) confirms the lower amount of Cu exposed on the surface for 15Cu-Sep, suggesting a poorer dispersion of available Cu species.

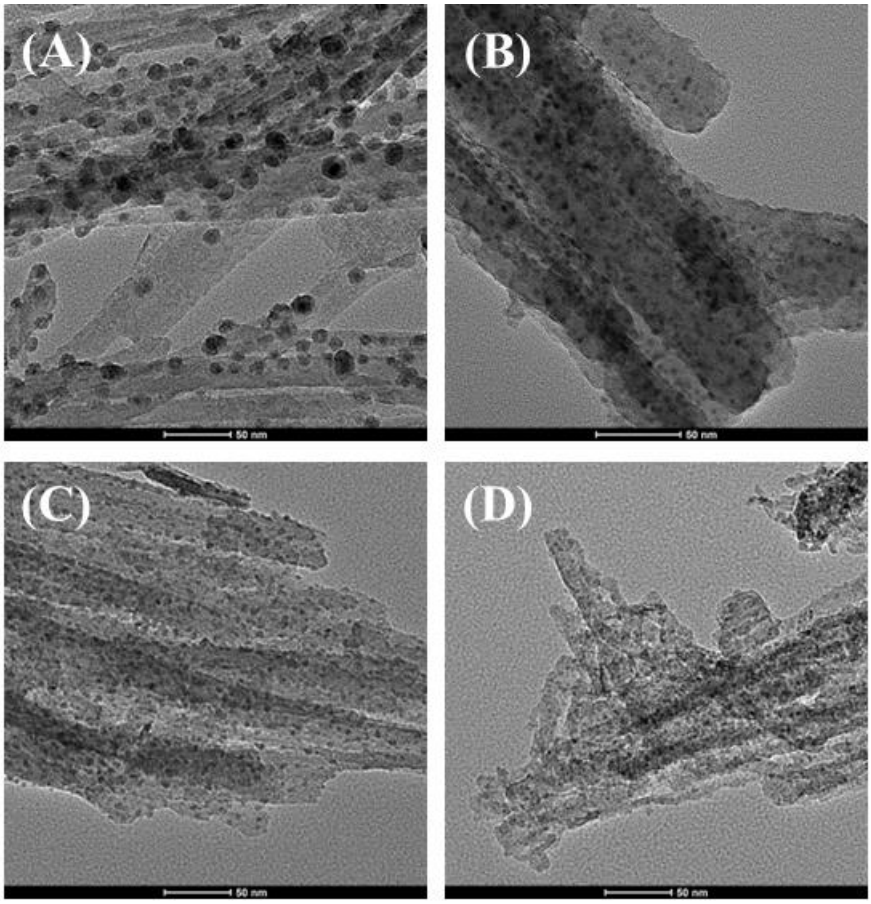


Figure 9. TEM micrographs of the Cu-based catalysts supported on raw sepiolite and sepiolite modified with microwave-assisted acid treatment at different times. 15Cu-Sep (**A**), 15Cu-Sep-2 (**B**), 15Cu-Sep-8 (**C**) and 15Cu-Sep-16 (**D**). Scale 50 nm.

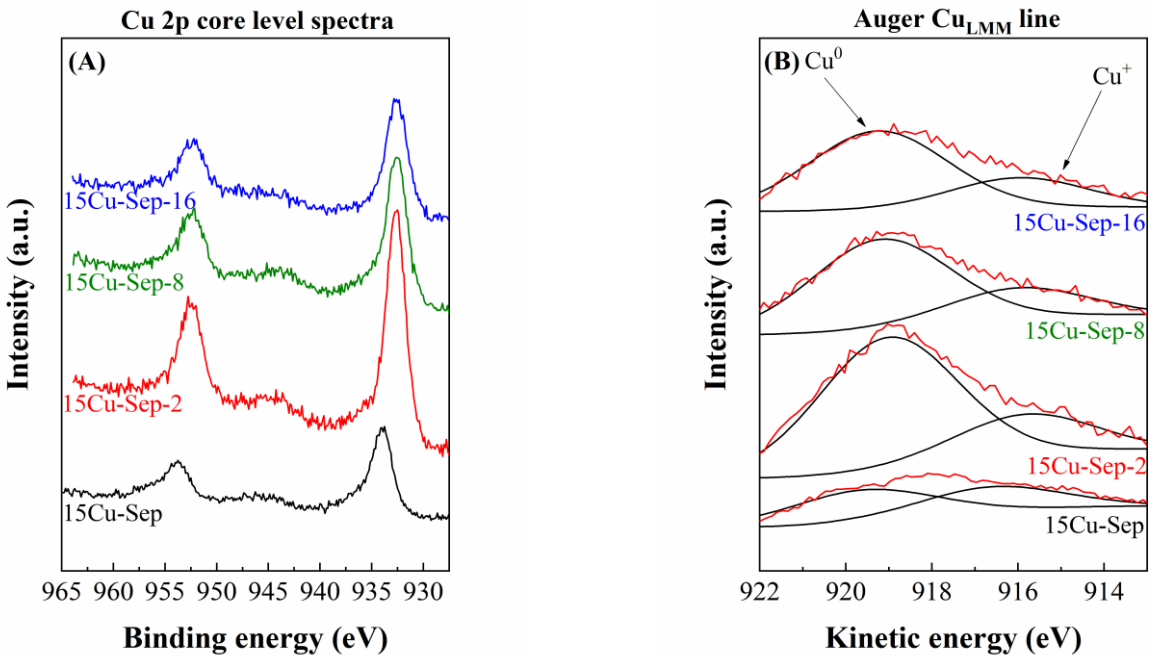


Figure 10. Cu 2p core level spectra (**A**) and Cu_{LMM} Auger line (**B**) of the Cu-based catalysts supported on raw sepiolite and sepiolite modified with microwave-assisted acid treatment at different times.

Table 2. Atomic concentrations on the surface obtained from the XPS spectra of the Cu-based catalysts supported on raw sepiolite and sepiolite modified with microwave-assisted acid treatment at different times.

Sample	Atomic Concentrations (%)					
	C 1s	O 1s	Mg 2p	Al 2s	Si 2p	Cu 2p
15Cu-Sep	22.54	45.66	9.13	4.33	17.40	0.29
15Cu-Sep-2	17.44	48.13	6.53	4.32	20.71	2.91
15Cu-Sep-8	13.21	53.36	4.22	4.35	22.02	2.85
15Cu-Sep-16	8.94	56.10	1.21	4.44	28.72	1.91

From the Cu 2p core level spectra, it is not possible to discern between the reduced Cu species (Cu^0 and Cu^+). However, the analysis of the Cu_{LMM} Auger line allows to differentiate between both reduced species (Figure 10B). The analysis of this region displays a main contribution located about 919 eV, which is assigned to the presence of Cu^0 species while the contribution with lower intensity, located around 916 eV, is attributed to the existence of Cu^+ species [34–36] although the H_2-TPR signals confirmed the total reduction in Cu species (Figure 7). Nevertheless, the presence of Cu^+ species can be considered beneficial for the FUR reaction since it could provide acid sites, which are involved in the hydrogenolysis of FOL to MF [63,64].

4. Catalytic Results

Once the Cu-based catalysts were characterized, the samples were assayed in gas-phase in the FUR hydrogenation to obtain valuable products. For this study cyclopenthyl methyl ether (CPME) was selected as solvent since this compound is considered environmentally friendly, being used in some biomass valorization reactions as the dehydration of xylans to obtain FUR [65]. The thermochemical stability of CPME was studied considering similar catalytic conditions to those performed in the gas-phase of FUR hydrogenation. The obtained results hardly show FUR conversion, discarding its reactivity in the catalytic conditions used in the present study.

In the first study, Cu-based catalysts (15 wt.% of Cu) supported in sepiolite, which was subjected to microwave-assisted acid treatment at different times, was studied in the FUR hydrogenation at 190 °C for 5 h (Figure 11A). Despite all catalysts displaying similar Cu content, the catalytic behavior is different between them, suggesting that the modification in the chemical composition of the support plays an important role in the catalytic behavior. Thus, the catalyst 15Cu-Sep catalyst achieves the lowest conversion values (51% after 1 h of reaction, decreasing this conversion until 34% after 5 h of reaction at 190 °C). The use of sepiolite modified under microwave-assisted acid treatment as support causes a clear improvement of the FUR conversion, reaching a full conversion after 1 h of reaction when the sepiolite is only treated for 2 min (15Cu-Sep-2 catalyst). In the same way, the deactivation is more limited along the time since 15Cu-Sep-2 catalyst still maintains a conversion of 93% after 5 h of reaction at 190 °C. However, the use of a support where sepiolite has been subjected to a longer acid treatment causes a progressively worsens in the catalytic behavior. Thus, 15Cu-Sep-16 catalyst shows a decrease in the FUR conversion from 88% after 1 h or reaction to 61% after 5 h of reaction at 190 °C. As was described in previous studies, the progressive decrease in the FUR conversion along the time on stream is attributed to the high reactivity of the FUR molecules since this molecule is prone to suffer polymerization reactions, mainly in gas-phase, causing a strong deactivation of the available active sites due to the deposition of carbonaceous deposits on the surface of the catalyst [34,35].

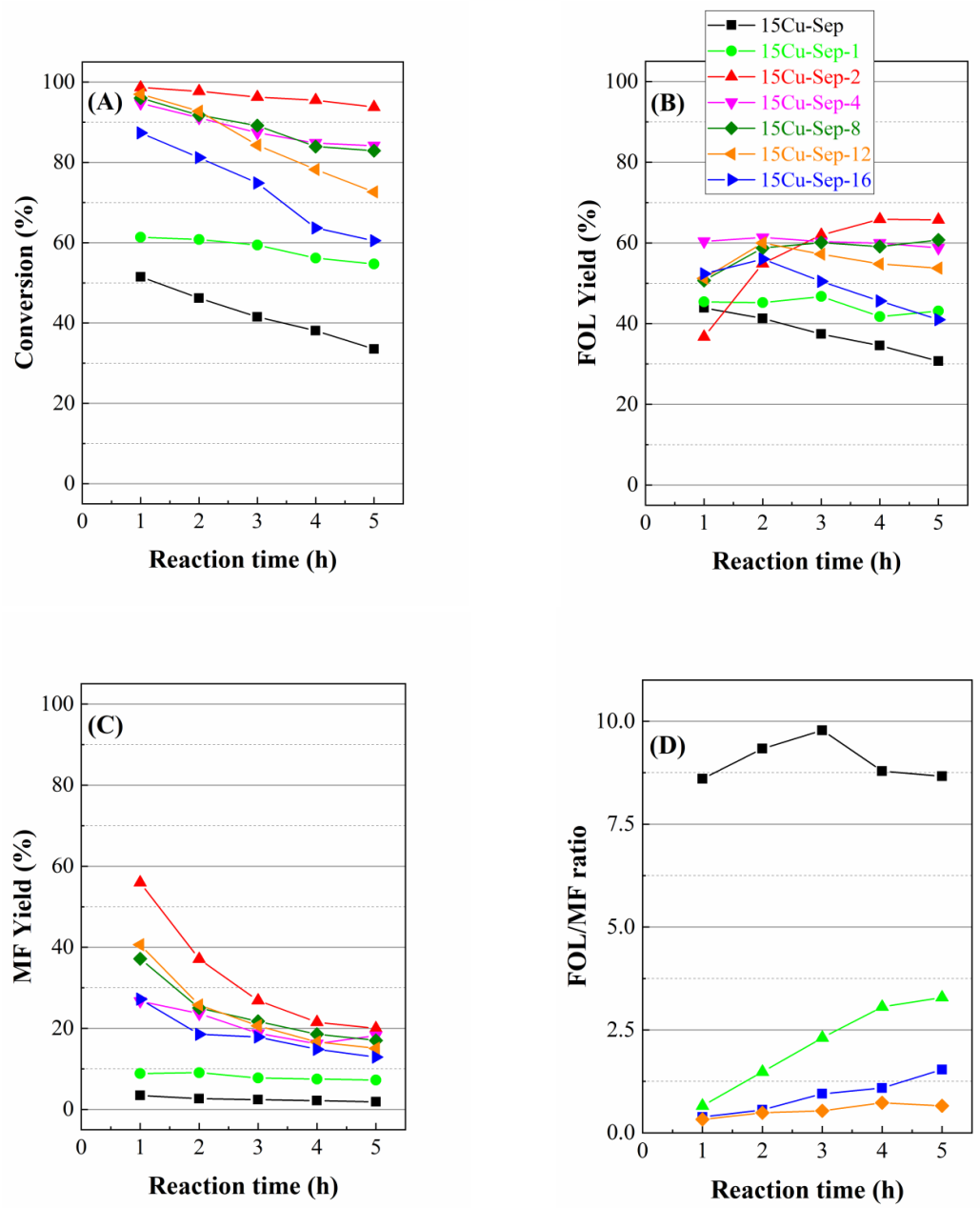


Figure 11. FUR conversion (**A**), FOL yield (**B**), MF yield (**C**) and FOL/MF molar ratio (**D**) the FUR hydrogenation in gas phase using Cu-based catalysts supported on sepiolite modified with an acid treatment. Experimental conditions: mass of catalyst = 0.15 g, reaction temperature = 190 °C, reaction time = 1–5 h, pressure = 0.1 MPa, H_2 flow = 10 mL/min, and feed flow = 2.3 mmol FUR/h.

The poorest catalytic behavior of the 15Cu-Sep sample attributed to this catalyst displays bigger metallic particles in comparison with other catalysts where sepiolite was subjected to microwave-assisted acid treatment. This implies a lower amount of Cu sites exposed on its surface (Figure 10 and Table 2). The acid treatment causes a progressive increase in the specific surface area of the support, which could promote a higher dispersion of the active phase due to the loss of the octahedral sheet by leaching of the Mg species. The characterization of these catalysts reported a smaller particle size of Cu^0 (Figure 9), which implies a higher dispersion of the available hydrogenating sites, promoting a higher conversion value. The presence of these smaller Cu^0 crystals is observed in all catalysts where the sepiolite is treated with acid treatment at different times. Despite the catalyst displaying an improvement in the textural properties, the use of longer acid treatment

promotes a deterioration of the catalytic behavior probably due to modifications in the interactions between metallic sites and support. In this sense, previous studies have reported that the presence of Mg species provides basic sites, which has a positive effect in the catalytic behavior [66,67]. Considering those catalysts where the crystal size of Cu^0 is similar and well dispersed, the catalytic results seem to indicate that the formation of catalysts with lower levels of Mg species worsens the catalytic behavior, so the presence of these Mg species seems to be a beneficial effect on the FUR conversion, as was observed in previous studies [68].

Regarding the selectivity pattern, furfuryl alcohol (FOL) and 2-methylfuran (MF) were the obtained products (Figure 11B,C). It is striking how the most active catalysts achieve higher proportions of MF in shorter times. However, the yield towards this product notably decreases along the time on stream. This decrease is accompanied by a progressive increase in the FOL content, which suggests the presence of consecutive reactions in these reaction conditions. Several studies have proposed the mechanism of this reaction. Thus, the first studies, carried out by Sitthisa et al., pointed out that the interaction between the Cu sites and FUR molecule to form FOL by a hydrogenation reaction takes place through the oxygen atom of the carbonyl group with a η^1-(O)-aldehyde configuration [27,69], which was confirmed by DFT studies later [28]. In a second step, FOL interacts with the active phase through the oxygen atom of the hydroxyl group to form MF via hydrogenolysis reaction [28]. This step requires acid sites although the acidity must be modulated since the presence of high number of acid sites with high strength promotes the formation of the humins, which causes a fast deactivation of the catalyst. In this sense, previous authors have pointed out that presence of low acidity can be enough to promote this hydrogenolysis reaction [30]. In the same way, the presence of small particles of Cu^0 particles as well as the presence of Cu^+-species can act as Lewis acid sites to promote the hydrogenolysis reaction [30,34,36]. The profile of MF and FOL yield suggests that the sites involved in the hydrogenolysis reaction (FOL → MF) are more prone to suffer deactivation in comparison to the sites involved in the hydrogenation reaction (FUR → FOL). Considering these premises, the catalytic results show how the catalyst with lower dispersion and bigger crystal size, i.e., 15Cu-Sep sample, hardly displays yield towards MF. These data agree with those reported in the literature since the presence of bigger Cu^0-crystals promotes the hydrogenation reaction (FUR → FOL) [36]. However, the presence of a higher dispersion of Cu^0 and the existence of Cu^+-species on the surface promotes the hydrogenolysis reaction (FOL → MF) [34,36]. Among the samples, the most active is 15Cu-Sep-2 catalyst, which achieves a MF yield of 56% after 1 h of reaction at 190 °C. The biggest MF yield can be ascribed to the higher amount of Cu species exposed on its surface as well as the presence of Mg species, which promotes an appropriate interaction active-phase support where the presence of collateral reaction and the formation of undesired by-products are minimized [34,68]. Nevertheless, the yield decreases notably until reaching a value of 20% after 5 h of reaction at 190 °C. This decrease is accompanied by a clear increase in the FOL yield, obtaining a maximum value of 65% after 5 h of reaction, as was indicated in Figure 11D. In summary, the crystal size of the Cu species (Cu^0 and Cu^+) has a determining role in the selectivity pattern since the catalyst with bigger crystal size tends to promote the hydrogenation reaction (FUR → FOL). However, the presence of smaller crystals are prone to the hydrogenation and a subsequent hydrogenolysis reaction to form MF (FUR → FOL → MF), although these sites are more sensitive to suffer deactivation processes in such a way the reaction is retained in the hydrogenation reaction and does not evolve towards MF, forming FOL as main product (Figure 11D).

As 15Cu-Sep-2 catalyst reached the highest activity and stability along the time on stream, this sample was selected to evaluate the influence of the reaction temperature in

the catalytic behavior (Figure 12A). These data show how FUR conversion decreases along the time when the reaction takes place at milder temperature (170 °C) from 78% after 1 h of reaction and to 63% after 5 h of reaction. The use of a higher temperature leads to almost full conversion along the time on stream. Despite this similar activity, the yields towards FOL and MF differ between them (Figure 12B,C). The analysis of the yields at shorter reaction times reveals that FOL is preferably formed at lower temperature, obtaining a maximum yield of 63% after 1 h when the reaction takes place at 170 °C. This trend is hardly modified along the time on stream since the reaction at 170 °C is very stable obtaining FOL as main product along the reaction (Figure 12D). However, the catalytic stability for the tests carried out at higher temperature is lower due to the yield towards MF decreases throughout the reaction while FOL levels increase (Figure 12D). From these data, it can be inferred that the hydrogenolysis reaction is promoted at higher temperatures although these sites are prone to be deactivated under these conditions along the reaction, remaining the reaction in hydrogenation of FUR to FOL.

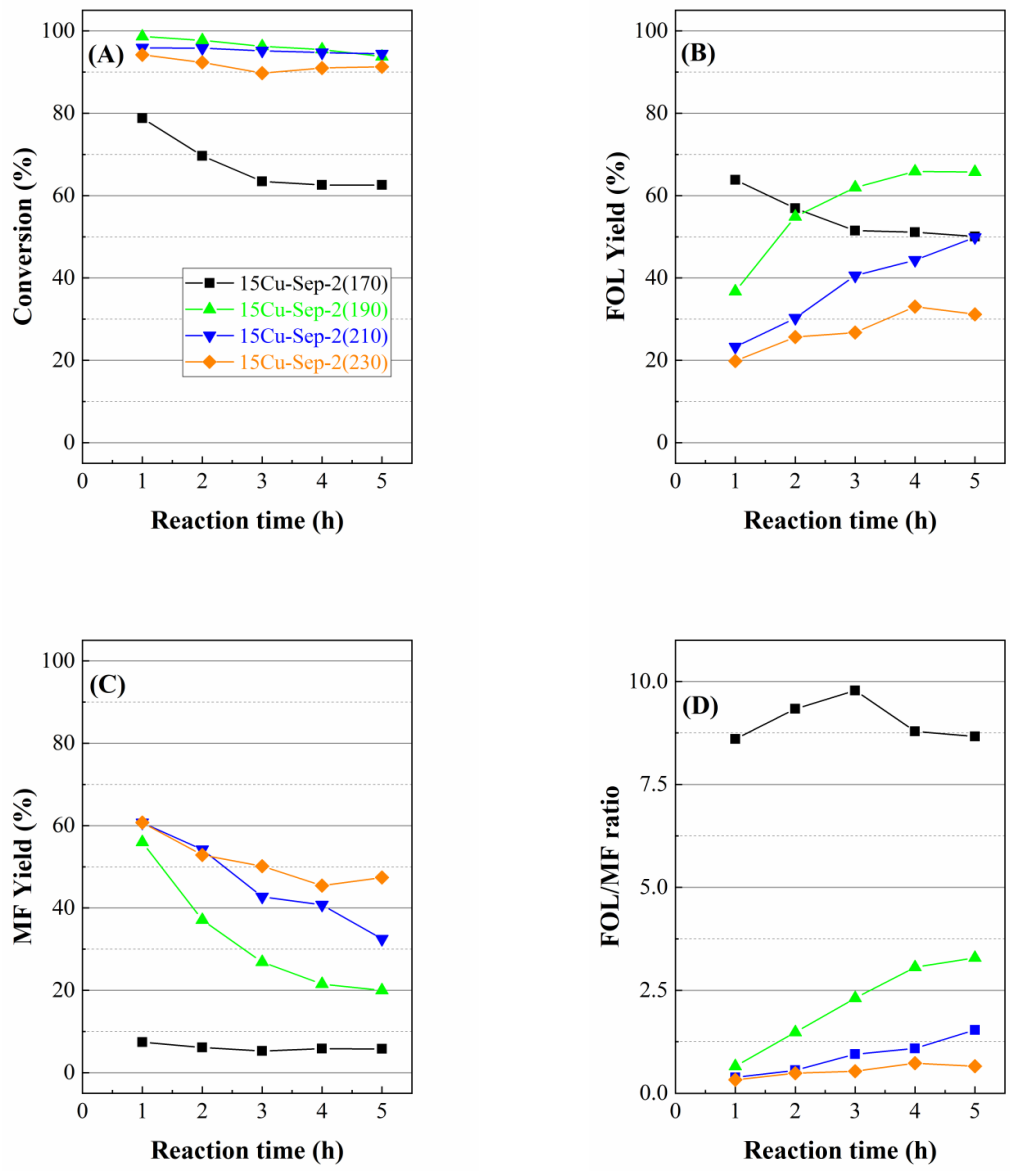


Figure 12. FUR conversion (**A**), FOL yield (**B**), MF yield (**C**) and FOL/MF molar ratio (**D**) in the FUR hydrogenation in gas phase using Cu-based catalysts supported on sepiolite modified with an acid treatment. Experimental conditions: mass of catalyst = 0.15 g, reaction temperature = 170–230 °C, reaction time = 1–5 h, pressure = 0.1 MPa, H_2 flow = 10 mL/min, and feed flow = 2.3 mmol FUR/h.

In a final catalytic study, the influence of Cu content was evaluated considering the best catalytic support (Sep-2) (Figure 13). Catalytic data reveal that the reaction is sensitive to the Cu content (Figure 13A). Thus, an increase in the Cu content causes a significant improvement in the catalytic behavior, since the 5Cu-Sep-2 and 10Cu-Sep-2 catalysts reach a conversion of 40% and 72%, respectively, after 1 h of reaction while the FUR conversion is practically complete along 5 h of reaction when the catalyst displays a Cu content higher than 15 wt.%. Regarding the obtained products (Figure 13B,C), a low Cu content promotes the hydrogenation of FUR to FOL although the conversion is poorer than that observed for other catalysts with higher Cu loading. However, those catalysts with a higher Cu content promote hydrogenation and a subsequent hydrogenolysis step to form MF. In fact, the data reported in Figure 13D shows how the 5Cu-Sep-2 catalyst, where the hydrogenation reaction towards FOL is promoted, maintains a more stable FOL/MF ratio along the time on stream. However, the catalysts with higher Cu content, which are more selective towards MF in shorter reaction times, modify the FOL/MF ratio along the time on stream. This confirms the faster deactivation of the hydrogenolysis sites.

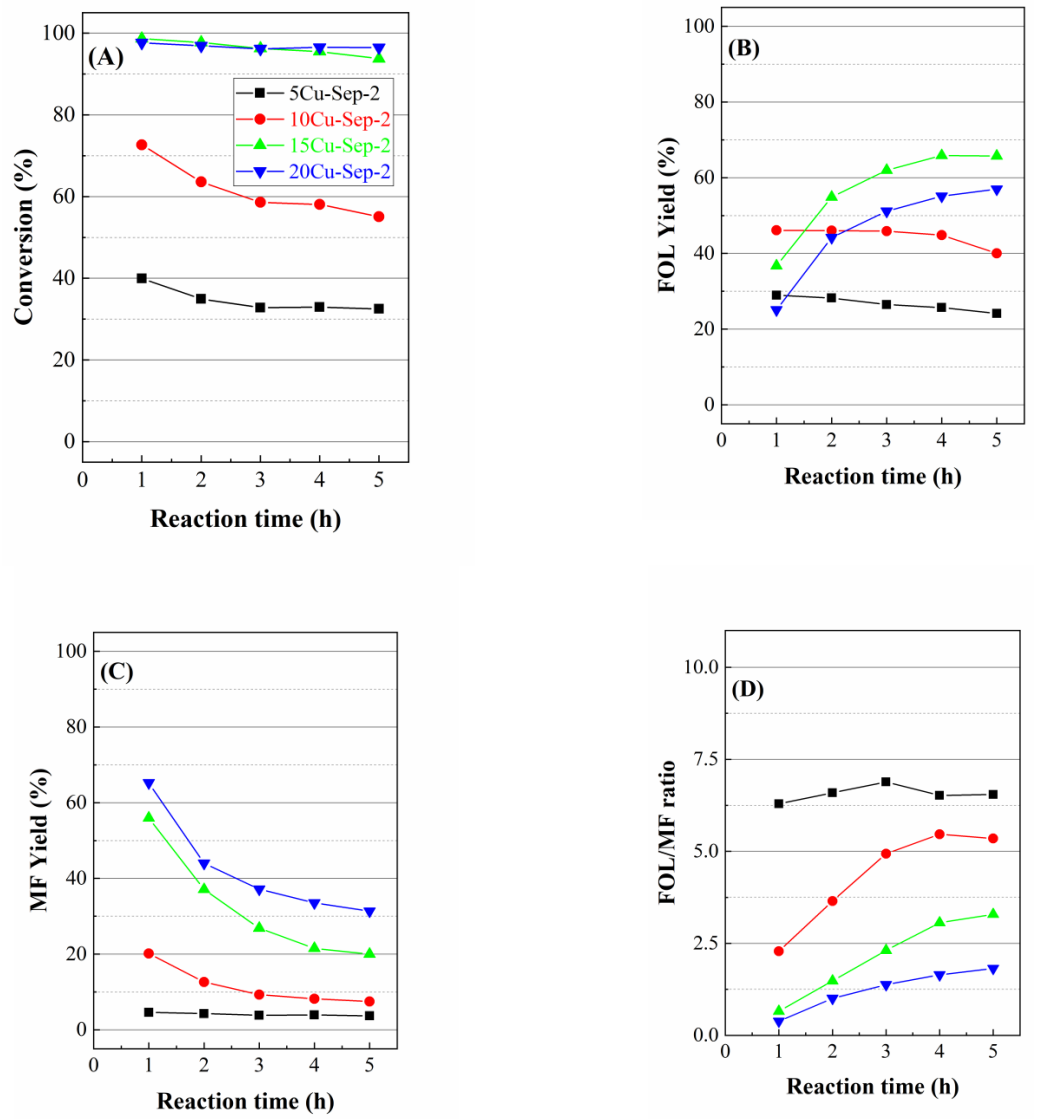


Figure 13. FUR conversion (**A**), FOL yield (**B**), MF yield (**C**) and FOL/MF molar ratio (**D**) in the FUR hydrogenation in gas phase using Cu-based catalysts supported on sepiolite modified with an acid treatment. Experimental conditions: mass of catalyst = 0.15 g, reaction temperature = 190 °C, reaction time = 1–5 h, pressure = 0.1 MPa, H_2 flow = 10 mL/min, and feed flow = 2.3 mmol FUR/h.

Finally, the catalysts with different Cu content supported on Sep-2 were characterized to understand the differences in the catalytic behavior. Firstly, the reducibility of the Cu-based precursors was analyzed by H_2-TPR (Figure 14A). These data reveal that the H_2-consumption increases with the Cu content, which is expected due to the reduction in a bigger amount of Cu^{2+}-species to Cu^0. However, the most representative data of these profiles is related to the similar temperature at which the maximum H_2-consumption takes place. This suggests that the interaction precursor-support hardly suffers modification when the content of the Cu incorporated is modified. The study of the samples with different Cu content by XRD (Figure 14B) reveals that all catalysts, except that sample with the highest Cu content, do not show any reflections lines ascribed to Cu species. In the case of 20Cu-Sep-2 sample, the main diffraction peak ascribed to Cu^0 is observed at 2θ (°) of 43.2 (PDF N°: 00-002-1225), although this signal is relatively wide in such a way that the metallic particles must be relatively small even for high Cu content (20 wt.%). This fact was confirmed by the analysis of their TEM micrographs (Figure 14C and Supplementary Material, Figure S11) since the particles are homogeneous and spherical with diameter lower than 5 nm in all catalysts, confirming the high dispersion of the active phase in all cases. The analysis of the samples by XPS (Figure 14D,E) reveals that the Cu exposed on the surface increases directly with the Cu content. In the same way, the analysis of the Cu 2p core level spectra show the existence of reduced Cu species in all catalysts exclusively (Figure 14D). The detailed analysis of the Cu_{LMM} Auger line displays the presence of two contributions (Figure 14E). The main contribution, located about 919 eV, is assigned to Cu^0 while the lower contribution about 916 eV is attributed to Cu^+ species [34,35]. Despite presenting the same contributions in the Cu regions, the ratio of products obtained is variable for the catalysts with different Cu loading. The results obtained suggest that the hydrogenolysis sites involved in the formation of MF seems to be deactivated more quickly. Thus, the lower proportion of hydrogenolysis sites in 5Cu-Sep-2 catalyst implies a faster deactivation of these sites in such a way this catalyst displays low proportion of MF while the FOL yield is more stable along the time on stream. On the opposite, the catalyst with higher amount of Cu exposed on the surface (Cu^0 and Cu^+), i.e., higher amount of hydrogenation and hydrogenolysis sites promotes the formation of MF during longer time although these sites are also prone to be deactivated along the time on stream, as indicates Figure 13D.

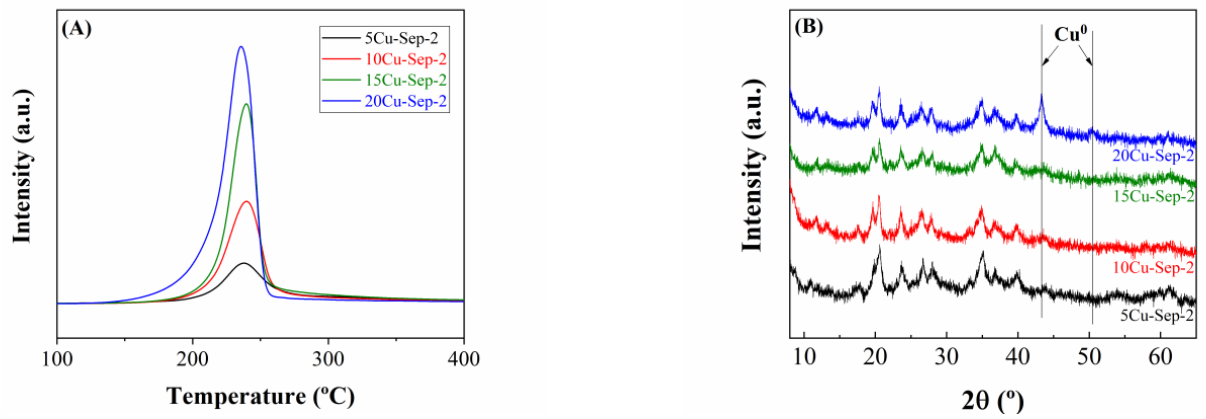


Figure 14. *Cont.*

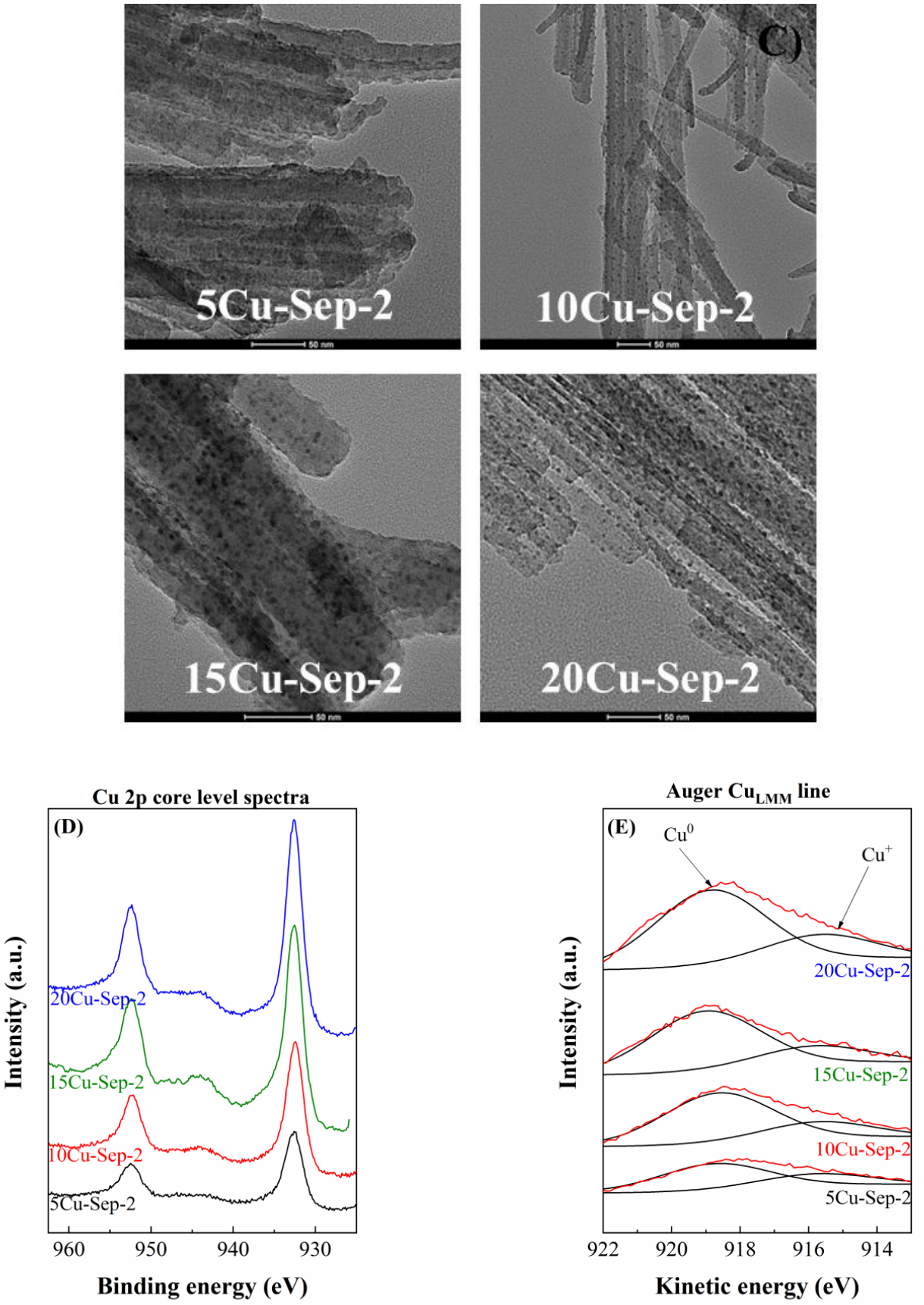


Figure 14. H_2-TPR profiles (**A**), X-ray diffractograms (**B**), TEM micrographs (Scale: 50 nm) (**C**), Cu 2p core level spectra (**D**) and Cu_{LMM} Auger line (**E**) of 5Cu-Sep-2, 10Cu-Sep-2, 15Cu-Sep-2 and 20Cu-Sep-2 catalysts.

5. Conclusions

In this work, a fibrous clay mineral, sepiolite, has been modified through a microwave-assisted acid treatment. This treatment has caused a progressive leaching of the Mg^{2+} species located in the octahedral layer, leading to an increase in the surface area and pore volume. These samples with different textural properties have been used as supports for the precipitation-deposition of Cu species on its surface. The characterization of the samples revealed that CuO particles were dispersed on the surface of the raw sepiolite, while $Cu_2(OH)_3{}^+$ species have been deposited over the sepiolite subjected to microwave-assisted acid treatment in these sites where Mg^{2+}-species were previously leached by the microwave-assisted acid treatment. These Cu species are highly dispersed on the surface of these modified supports even after calcination and reduction treatment, obtaining Cu^0 particles with a size less than 5 nm. In contrast, the Cu^0 particles supported on raw sepiolite display a much larger particle size between 15 and 25 nm.

Once the materials were characterized, the samples were assayed in the gas phase hydrogenation of furfural. Generally, the difference in Cu^0 crystal size was reflected in its catalytic behavior. These results showed that the catalyst with a larger Cu^0 crystal size (15Cu-Sep) is selective to the hydrogenation reaction, obtaining FOL as main product. However, the catalysts where the sepiolite was subjected to different microwave-assisted acid treatments and smaller Cu^0 particle size are more active and promote two consecutive reactions. Firstly, FOL is obtained through a hydrogenation reaction of FUR. In a second step, MF is obtained from a hydrogenolysis reaction of FOL through mild acid sites. Between the two reactions, the catalytic results indicated that the sites involved in the hydrogenolysis reaction are more prone to be deactivated, while the sites involved in the hydrogenation reaction are more resistant to deactivation although these sites are less active.

The results obtained reveal that the presence of small Cu crystals has a determining role in the catalytic behavior. However, the use of short acid treatment times, where a proportion of Mg^{2+}-species remain in the fibrous structure, also has a positive effect in the catalytic behavior, since the presence of Mg in the support also has a positive effect on the FUR hydrogenation reaction in gas phase.

Supplementary Materials: The following supporting information can be downloaded at: https://www.mdpi.com/article/10.3390/ceramics8010021/s1, Table S1. Chemical composition of the raw sepiolite and sepiolite subjected at different times of microwave-assisted acid treatment; Table S2. Atomic concentrations on the surface obtained from the XPS spectra for the raw sepiolite and sepiolite subjected at different times of microwave-assisted acid treatment with Cu-species deposited on its surface; Figure S1. N_2 adsorption-desorption isotherms of the raw sepiolite and sepiolite subjected at different times of microwave-assisted acid treatment; Figure S2. Pore size distribution of the raw sepiolite and sepiolite subjected at different times of microwave-assisted acid treatment; Figure S3. Zeta potential of the raw sepiolite and sepiolite subjected at different times of microwave-assisted acid treatment; Figure S4. X-Ray diffractogram of the solid obtained after the treatment of $Cu(NO_3)_2$ $3H_2O$ in urea solution at 95 °C; Figure S5. N 1s core level spectra of the raw sepiolite and sepiolite subjected at different times of microwave-assisted acid treatment with Cu-species deposited on its surface (estimated by XPS); Figure S6. Images of Prec-15CuO-Sep (A), Prec-15CuO-Sep-2 (B), Prec-15CuO-Sep-8 (C) and Prec-15CuO-Sep-16 (D); Figure S7. Images of 15CuO-Sep (A), 15CuO-Sep-2 (B), 15CuO-Sep-8 (C) and 15CuO-Sep-16 (D); Figure S8. Method of band gap energy (eV) determination from theTauc plot of the raw sepiolite and sepiolite subjected at different times of microwave-assisted acid treatment with Cu-species deposited on its surface; Figure S9. EDX mapping of the Cu-based catalysts supported on raw sepiolite and sepiolite modified with microwave-assisted acid treatment at different times. 15Cu-Sep (A), 15Cu-Sep-2 (B), 15Cu-Sep-8 (C) and 15Cu-Sep-16 (D). Scale 100 nm; Figure S10. Distribution of the Cu crystals for 15Cu-Sep, 15Cu-Sep-2, 15Cu-Sep-8 and 15Cu-Sep-16;

Figure S11. EDX mapping of the Cu-based catalysts supported on raw sepiolite and sepiolite modified with microwave-assisted acid treatment at different times. 5Cu-Sep (A), 10Cu-Sep-2 (B), 15Cu-Sep-2 (C) and 20Cu-Sep-2 (D). Scale 100 nm.

Author Contributions: Conceptualization, J.A.C. and P.J.M.-T.; methodology, J.A.C., R.M.-T. and P.J.M.-T.; software, A.G.-T., R.M.-S. and J.A.C.; validation, J.A.C., R.M.-T. and C.G.-S.; formal analysis, A.G.-T., R.M.-S. and J.A.C.; investigation, A.G.-T., R.M.-S. and J.A.C.; resources, R.M.-T. and P.J.M.-T.; data curation, J.A.C., R.M.-T., J.J.Q.-S. and C.G.-S.; writing—original draft preparation, J.A.C.; writing—review and editing, J.A.C., C.G.-S. and P.J.M.-T.; visualization, J.A.C.; supervision, J.J.Q.-S., R.M.-T., P.J.M.-T.; project administration, R.M.-T. and P.J.M.-T.; funding acquisition, R.M.-T. and P.J.M.-T. All authors have read and agreed to the published version of the manuscript.

Funding: This research was funded by the Spanish Ministry of Science and Innovation (PID2021-122736OB-C42) and FEDER (European Union) funds.

Institutional Review Board Statement: Not applicable.

Informed Consent Statement: Not applicable.

Data Availability Statement: The data presented in this study are available on request from the corresponding author.

Acknowledgments: The authors thank Servicio Central de Apoyo a la Investigación (SCAI—Universidad de Málaga) for its availability in the characterization. The authors also thank Tolsa to supply the starting sepiolite.

Conflicts of Interest: The authors declare no conflicts of interest.

References

1. Bian, Z.; Kawi, S. Preparation, characterization and catalytic application of phyllosilicate: A review. *Catal. Today* **2020**, *339*, 3–23. [CrossRef]
2. Ruíz, A.I.; Ruíz-García, C.; Ruíz-Hitzky, E. From old to new inorganic materials for advanced applications: The paradigmatic example of the sepiolite clay mineral. *Appl. Clay Sci.* **2023**, *235*, 106874. [CrossRef]
3. Galán, E.; Pozo, M. Palygorskite and sepiolite deposits in continental environments. description, genetic patterns and sedimentary settings. *Develop. Clay Sci.* **2011**, *3*, 125–173. [CrossRef]
4. Suárez, M.; García-Romero, E. Advances in the crystal chemistry of sepiolite and palygorskite. *Dev. Clay Sci.* **2011**, *3*, 33–65. [CrossRef]
5. Jones, B.F.; Galán, E. Sepiolite and palygorskite. *Rev. Mineral.* **1988**, *19*, 631–674. [CrossRef]
6. Cecilia, J.A.; Vilarrasa-García, E.; Cavalcante, C.L., Jr.; Azevedo, D.C.S.; Franco, F.; Rodríguez-Castellón, E. Evaluation of two fibrous clay minerals (sepiolite and palygorskite) for CO_2 capture. *J. Environ. Chem. Eng.* **2018**, *6*, 4573–4587. [CrossRef]
7. Álvarez, A. Sepiolite: Properties and uses. *Dev. Sedimentol.* **1984**, *37*, 253–287. [CrossRef]
8. Song, N.; Hursthouse, A.; McLellan, I.; Wang, Z. Treatment of environmental contamination using sepiolite: Current approaches and future potential. *Environ. Geochem. Health* **2021**, *43*, 2679–2697. [CrossRef]
9. Hamid, Y.; Tang, L.; Hussain, B.; Usman, M.; Liu, L.; Ulhassan, Z.; He, Z.; Yang, X. Sepiolite clay: A review of its applications to immobilize toxic metals in contaminated soils and its implications in soil–plant system. *Environ. Technol. Innov.* **2021**, *23*, 101598. [CrossRef]
10. Biddeci, G.; Spinelli, G.; Colomba, P.; Di Blasi, F. Halloysite nanotubes and sepiolite for health applications. *Int. J. Mol. Sci.* **2023**, *24*, 4801. [CrossRef]
11. Tang, Y.; Yang, D.; Ting, V.P.; Hamerton, I.; Van Duijneveldt, J.S.; Rochat, S. Modified sepiolite nanoclays in advanced composites for engineering applications. *ACS Appl. Nano Mater.* **2024**, *7*, 19221–19232. [CrossRef] [PubMed]
12. Franco, F.; Pozo, M.; Cecilia, J.A.; Benítez-Guerrero, M.; Pozo, E.; Martín Rubí, J.A. Microwave assisted acid treatment of sepiolite: The role of composition and "crystallinity". *Appl. Clay Sci.* **2014**, *102*, 15–27. [CrossRef]
13. Jiménez-López, A.; López-González, J.D.; Ramírez-Sáenz, A.; Rodríguez-Reinoso, F.; Valenzuela-Calahorro, C.; Zurita-Herrera, L. Evolution of surface area in a sepiolite as a function of acid and heat treatments. *Clay Miner.* **1978**, *13*, 375–385. [CrossRef]
14. Balci, S. Effect of heating and acid pre-treatment on pore size distribution of sepiolite. *Clay Miner.* **1999**, *34*, 647–655. [CrossRef]
15. Yebra-Rodríguez, A.; Martín-Ramos, J.D.; del Rey, F.; Viseras, C.; López-Galindo, A. Effect of acid treatment on the structure of sepiolite. *Clay Miner.* **2003**, *38*, 353–360. [CrossRef]

16. Surendra, B.S.; Veerabhadraswamy, M.; Kumar, H.G.A.; Kendagannaswamy, B.K.; Nagaswarupa, H.P.; Prashanth, S.C. Microwave assisted physico-chemical modification of Bentonite clay: Characterization and photocatalytic activity. *Mater. Today* **2017**, *4*, 11727–11736. [CrossRef]
17. Wu, C.R.; Hong, Z.Q.; Zhan, B.J.; Tang, W.; Cui, S.C.; Kou, S.C. Effect of acid treatment on the reactivity of natural sepiolite used as a supplementary cementitious material. *Constr. Build. Mater.* **2022**, *316*, 125860. [CrossRef]
18. Jaswal, A.; Singh, P.P.; Mondal, T. Furfural—A versatile, biomass-derived platform chemical for the production of renewable chemicals. *Green Chem.* **2022**, *24*, 510–551. [CrossRef]
19. Yong, K.J.; Wu, T.Y.; Lee, C.B.T.L.; Lee, Z.J.; Liu, Q.; Jahim, J.M.; Zhou, Q.; Zhang, L. Furfural production from biomass residues: Current technologies, challenges and future prospects. *Biomass Bioenergy* **2022**, *161*, 106458. [CrossRef]
20. Jatoi, A.S.; Abbasi, S.A.; Hashmi, Z.; Shah, A.K.; Alam, M.S.; Bhatti, Z.A.; Maitlo, G.; Hussain, S.; Khandro, G.A.; Usto, M.A.; et al. Recent trends and future perspectives of lignocellulose biomass for biofuel production: A comprehensive review. *Biomass Conv. Bioref.* **2023**, *13*, 6457–6469. [CrossRef]
21. Adhami, W.; Richel, A.; Len, C. A review of recent advances in the production of furfural in batch system. *Mol. Catal.* **2023**, *545*, 113178. [CrossRef]
22. Wang, Y.; Zhao, D.; Rodríguez-Padrón, D.; Len, C. Recent advances in catalytic hydrogenation of furfural. *Catalysts* **2019**, *9*, 796. [CrossRef]
23. Adkins, H.; Connor, R. The catalytic hydrogenation of organic compounds over copper chromite. *J. Am. Chem. Soc.* **1931**, *53*, 1091–1095. [CrossRef]
24. Rao, R.; Dandekar, A.; Baker, R.T.K.; Vannice, M.A. Properties of copper chromite catalysts in hydrogenation reactions. *J. Catal.* **1997**, *171*, 406–419. [CrossRef]
25. Liu, D.; Zemlyanov, D.; Wu, T.; Lobo-Lapidus, R.J.; Dumesic, J.A.; Miller, J.T.; Marshall, C.L. Deactivation mechanistic studies of copper chromite catalyst for selective hydrogenation of 2-furfuraldehyde. *J. Catal.* **2013**, *299*, 336–345. [CrossRef]
26. Zhang, H.; Lei, Y.; Kropf, A.J.; Zhang, G.; Elam, J.W.; Miller, J.T.; Sollberger, F.; Ribeiro, F.; Akatay, M.C.; Stach, E.A.; et al. Enhancing the stability of copper chromite catalysts for the selective hydrogenation of furfural using ALD overcoating. *J. Catal.* **2014**, *317*, 284–292. [CrossRef]
27. Sitthisa, S.; Sooknoi, T.; Ma, Y.; Balbuena, P.B.; Resasco, D.E. Kinetics and mechanism of hydrogenation of furfural on Cu/SiO_2 catalysts. *J. Catal.* **2011**, *277*, 1–13. [CrossRef]
28. Shi, Y.; Zhu, Y.; Li, Y.W.; Jiao, H. Exploring furfural catalytic conversion on Cu(111) from computation. *ACS Catal.* **2015**, *5*, 4020–4032. [CrossRef]
29. Yan, K.; Wu, G.; Lafleur, T.; Jarvis, C. Production, properties and catalytic hydrogenation of furfural to fuel additives and value-added chemicals. *Renew. Sustain. Energy Rev.* **2014**, *38*, 663–676. [CrossRef]
30. Dong, F.; Zhu, Y.; Zheng, H.; Zhu, Y.; Li, X.; Li, Y. Cr-free Cu-catalysts for the selective hydrogenation of biomass-derived furfural to 2-methylfuran: The synergistic effect of metal and acid sites. *J. Mol. Catal. A Chem.* **2015**, *398*, 140–148. [CrossRef]
31. Jiménez-Gómez, C.P.; Cecilia, J.A.; Durán-Martín, D.; Moreno-Tost, R.; Santamaría-González, J.; Mérida-Robles, J.; Mariscal, R.; Maireles-Torres, P. Gas-phase hydrogenation of furfural to furfuryl alcohol over Cu/ZnO catalysts. *J. Catal.* **2016**, *336*, 107–115. [CrossRef]
32. Nagaraja, B.M.; Kumar, V.S.; Shasikala, V.; Padmasri, A.H.; Sreedhar, S.; Raju, B.D.; Rao, K.S.R. A highly efficient Cu/MgO catalyst for vapour phase hydrogenation of furfural to furfuryl alcohol. *Catal. Commun.* **2003**, *4*, 287–293. [CrossRef]
33. Yang, X.; Chen, H.; Meng, Q.; Zheng, H.; Zhu, Y.; Li, Y.W. Insights into influence of nanoparticle size and metal–support interactions of Cu/ZnO catalysts on activity for furfural hydrogenation. *Catal. Sci. Technol.* **2017**, *7*, 5625–5634. [CrossRef]
34. Jiménez-Gómez, C.P.; Cecilia, J.A.; Moreno-Tost, R.; Maireles-Torres, P. Selective production of 2-methylfuran by gas-phase hydrogenation of furfural on copper incorporated by complexation in mesoporous silica catalysts. *ChemSusChem* **2017**, *10*, 1448–1459. [CrossRef]
35. Jiménez-Gómez, C.P.; Cecilia, J.A.; Alba-Rubio, A.C.; Cassidy, A.; Moreno-Tost, R.; García-Sancho, C.; Maireles-Torres, P. Tailoring the selectivity of Cu-based catalysts in the furfural hydrogenation reaction: Influence of the morphology of the silica support. *Fuel* **2022**, *319*, 123827. [CrossRef]
36. García-Sancho, C.; Mérida-Robles, J.M.; Cecilia-Buenestado, J.A.; Moreno-Tost, R.; Maireles-Torres, P.J. The role of copper in the hydrogenation of furfural and levulinic acid. *Int. J. Mol. Sci.* **2023**, *24*, 2443. [CrossRef]
37. Franco, F.; Pozo, M.; Cecilia, J.A.; Benítez-Guerrero, M.; Lorente, M. Effectiveness of microwave assisted acid treatment on dioctahedral and trioctahedral smectites. The influence of octahedral composition. *Appl. Clay Sci.* **2016**, *120*, 70–80. [CrossRef]
38. Korichi, S.; Elias, A.; Mefti, A. Characterization of smectite after acid activation with microwave irradiation. *Appl. Clay Sci.* **2009**, *42*, 432–438. [CrossRef]
39. Pardo, L.; Cecilia, J.A.; López-Moreno, C.; Hernández, V.; Pozo, M.; Bentabol, M.J.; Franco, F. Influence of the structure and experimental surfaces modifications of 2:1 clay minerals on the adsorption properties of methylene blue. *Minerals* **2018**, *8*, 359. [CrossRef]

40. Myriam, M.; Suárez, M.; Martín-Pozas, J.M. Structural and textural modifications of palygorskite and sepiolite under acid treatment. *Clays Clay Miner.* **1998**, *46*, 225–231. [CrossRef]
41. Frost, R.L.; Locos, O.B.; Ruan, H.; Kloprogge, J.T. Near-infrared and mid-infrared spectroscopic study of sepiolites and palygorskites. *Vib. Spectrosc.* **2001**, *27*, 1–13. [CrossRef]
42. Vilarrasa-García, E.; Cecilia, J.A.; Moura, P.A.S.; Azevedo, D.C.S.; Rodríguez-Castellón, E. Assessing CO_2 adsorption on amino-functionalized mesocellular foams synthesized at different aging temperatures. *Front. Chem.* **2020**, *8*, 591766. [CrossRef]
43. Thommes, M.; Kaneko, K.; Neimark, A.V.; Olivier, J.P.; Rodríguez-Reinoso, F.; Rouquerol, J.; Sing, K.S.W. Physisorption of gases, with special reference to the evaluation of surface area and pore size distribution (IUPAC Technical Report). *Pure Appl. Chem.* **2015**, *87*, 1051–1069. [CrossRef]
44. Brunauer, S.; Emmett, P.H.; Teller, E. Adsorption of gases in multimolecular layers. *J. Am. Chem. Soc.* **1938**, *60*, 309–319. [CrossRef]
45. Komadel, P. Acid activated clays: Materials in continuous demand. *Appl. Clay Sci.* **2016**, *131*, 84–99. [CrossRef]
46. Guerrero-Torres, A.; Jiménez-Gómez, C.P.; Cecilia, J.A.; García-Sancho, C.; Franco, F.; Quirante-Sánchez, J.J.; Maireles-Torres, P. Ni supported on sepiolite catalysts for the hydrogenation of furfural to value-added chemicals: Influence of the synthesis method on the catalytic performance. *Top. Catal.* **2019**, *62*, 535–550. [CrossRef]
47. Sarmet, J.; Taviot-Gheho, C.; Thirouard, R.; Leroux, F.; Douard, C.; Gaalich, I.; Brousse, T.; Toussaint, G.; Stevens, P. Electrochemical behavior of morphology-controlled copper (II) hydroxide nitrate nanostructures. *Cryst. Growth Des.* **2023**, *23*, 2634–2643. [CrossRef]
48. Luo, Y.H.; Huang, J.; Jin, J.; Peng, X.; Schmitt, W.; Ichinose, I. Formation of positively charged copper hydroxide nanostrands and their structural characterization. *Chem. Mater.* **2006**, *18*, 1795–1802. [CrossRef]
49. Van der Grift, C.J.G.; Elberse, P.A.; Mulder, A.; Geus, J.W. Preparation of silica-supported copper catalysts by means of deposition-precipitation. *Appl. Catal.* **1990**, *59*, 275–289. [CrossRef]
50. Lee, S.H.; Her, Y.S.; Matijevic, E. Preparation and growth mechanism of uniform colloidal copper oxide by the controlled double-jet precipitation. *J. Colloid Interface Sci.* **1997**, *186*, 193–202. [CrossRef]
51. Toupance, T.; Kermarec, M.; Lambert, J.F.; Louis, C. Conditions of formation of copper phyllosilicates in silica-supported copper catalysts prepared by selective adsorption. *J. Phys. Chem. B* **2002**, *106*, 2277–2286. [CrossRef]
52. Toupance, T.; Kermarec, M.; Louis, C. Metal particle size in silica-supported copper catalysts. Influence of the conditions of preparation and of thermal pretreatments. *J. Phys. Chem. B* **2000**, *104*, 965–972. [CrossRef]
53. Trouillet, L.; Toupance, T.; Villain, F.; Louis, C. In situ characterization of the coordination sphere of CuII complexes supported on silica during the preparation of Cu/SiO_2 catalysts by cation exchange. *Phys. Chem. Chem. Phys.* **2000**, *2*, 2005–2014. [CrossRef]
54. Zhang, G.; Long, J.; Wang, X.; Zhang, Z.; Dai, W.; Liu, P.; Li, Z.; Wu, L.; Fu, X. Catalytic role of Cu sites of Cu/MCM-41 in phenol hydroxylation. *Langmuir* **2010**, *26*, 1362–1371. [CrossRef]
55. Gomulka, A.; Iwaszko, O.; Kowalczyk, A.; Piwowarska, Z.; Rutkowska, M.; Chmielarz, L. Catalytic functionalization of MCM-41 and MCM-48 with copper by modified template ion-exchange method for low-temperature NH_3-SCR process: The role of complexing agents for copper dispersion. *Res. Chem. Intermed.* **2024**, *50*, 5399–5426. [CrossRef]
56. Giordano, F.; Vennestrøm, P.N.R.; Lundegaard, L.F.; Stappen, F.N.; Mossin, S.; Beato, P.; Bordiga, S.; Lamberti, C. Characterization of Cu-exchanged SSZ-13: A comparative FTIR, UV-Vis, and EPR study with Cu-ZSM-5 and Cu-β with similar Si/Al and Cu/Al ratios. *Dalton Trans.* **2013**, *42*, 12741–12761. [CrossRef]
57. Bezerra, S.M.; Levchenko, V.; Piccinelli, V.; Bettinelli, M.; Longo, R.L.; Malta, O.L.; Reisfeld, R. Amplification of light emission of lanthanide complexes by copper and copper oxide nanoparticles. *J. Lumin.* **2022**, *251*, 119217. [CrossRef]
58. Yin, A.; Guo, X.; Dai, W.L.; Li, H.; Fan, K. Highly active and selective copper-containing HMS catalyst in the hydrogenation of dimethyl oxalate to ethylene glycol. *Appl. Catal. A Gen.* **2008**, *31*, 91–99. [CrossRef]
59. Di, W.; Cheng, J.; Tian, S.; Li, J.; Chen, J.; Sun, Q. Synthesis and characterization of supported copper phyllosilicate catalysts for acetic ester hydrogenation to ethanol. *Appl. Catal. A Gen.* **2016**, *510*, 244–259. [CrossRef]
60. Ye, R.P.; Lin, L.; Yang, J.X.; Sun, M.L.; Li, F.; Li, B.; Yao, Y.G. A new low-cost and effective method for enhancing the catalytic performance of $Cu–SiO_2$ catalysts for the synthesis of ethylene glycol via the vapor-phase hydrogenation of dimethyl oxalate by coating the catalysts with dextrin. *J. Catal.* **2017**, *350*, 122–132. [CrossRef]
61. Arango-Díaz, A.; Cecilia, J.A.; Moretti, E.; Talon, A.; Núñez, P.; Marrero-Jerez, J.; Jiménez-Jiménez, J.; Jiménez-López, A.; Rodríguez-Castellón, E. Comparative study of CuO supported on CeO_2, $Ce_{0.8}Zr_{0.2}O_2$ and $Ce_{0.8}Al_{0.2}O_2$ based catalysts in the CO-PROX reaction. *Int. J. Hydrogen Energy* **2014**, *39*, 4102–4108. [CrossRef]
62. Ayastuy, J.L.; Gurbani, A.; González-Marcos, M.P.; Gutiérrez-Ortiz, M.A. Selective CO oxidation in H_2 streams on $CuO/Ce_xZr_{1-x}O_2$ catalysts: Correlation between activity and low temperature reducibility. *Int. J. Hydrogen Energy* **2012**, *37*, 1993–2006. [CrossRef]
63. Xia, Z.; Li, Y.; Wu, J.; Huang, Y.C.; Zhao, W.; Lu, Y.; Pan, Y.; Yue, X.; Wang, Y.; Dong, C.L.; et al. Promoting the electrochemical hydrogenation of furfural by synergistic Cu^0-Cu^+ active sites. *Sci. China Chem.* **2022**, *65*, 2588–2595. [CrossRef]

64. Zhang, J.; Ding, G.; Jin, Y.; Wei, L.; Li, X.; Wang, D.; Zhu, Y.; Li, Y. Stabilizing the interfacial Cu^0-Cu^+ dual sites toward furfural hydrodeoxygenation to 2-methylfuran via fabricating nest-like copper phyllosilicate precursor. *Fuel* **2023**, *337*, 127212. [CrossRef]
65. Campos Molina, M.J.; Mariscal, R.; Ojeda, M.; López Granados, M. Cyclopentyl methyl ether: A green co-solvent for the selective dehydration of lignocellulosic pentoses to furfural. *Bioresour. Technol.* **2012**, *126*, 321–327. [CrossRef]
66. Nagaraja, B.M.; Padmasri, A.H.; David Raju, B.; Rama Rao, K.S. Vapor phase selective hydrogenation of furfural to furfuryl alcohol over Cu–MgO coprecipitated catalysts. *J. Mol. Catal. A Chem.* **2007**, *265*, 90–97. [CrossRef]
67. Ghashghaee, M.; Sadjadi, S.; Shirvani, S.; Farzaneh, V. A novel consecutive approach for the preparation of Cu-MgO catalysts with high activity for hydrogenation of furfural to furfuryl alcohol. *Catal. Lett.* **2017**, *147*, 318–327. [CrossRef]
68. Guerrero-Torres, A.; Jiménez-Gómez, C.P.; Cecilia, J.A.; García-Sancho, C.; Quirante-Sánchez, J.J.; Mérida-Robles, J.M.; Maireles-Torres, P. Influence of the incorporation of basic or amphoteric oxides on the performance of Cu-based catalysts supported on sepiolite in furfural hydrogenation. *Catalysts* **2019**, *9*, 315. [CrossRef]
69. Sitthisa, S.; Resasco, D.E. Hydrodeoxygenation of furfural over supported metal catalysts: A comparative study of Cu, Pd and Ni. *Catal. Lett.* **2011**, *141*, 784–791. [CrossRef]

Disclaimer/Publisher's Note: The statements, opinions and data contained in all publications are solely those of the individual author(s) and contributor(s) and not of MDPI and/or the editor(s). MDPI and/or the editor(s) disclaim responsibility for any injury to people or property resulting from any ideas, methods, instructions or products referred to in the content.